



Published in final edited form as:

*Clin Cancer Res.* 2024 May 01; 30(9): 1859–1877. doi:10.1158/1078-0432.CCR-23-3841.

## Mesothelin CAR T-cells secreting anti-FAP/anti-CD3 molecules efficiently target pancreatic adenocarcinoma and its stroma

Marc Wehrli<sup>1,2,†</sup>, Samantha Guinn<sup>3,4,†</sup>, Filippo Birocchi<sup>1,2,†</sup>, Adam Kuo<sup>1,2</sup>, Yi Sun<sup>2</sup>, Rebecca C. Larson<sup>1,2</sup>, Antonio J. Almazan<sup>1,2</sup>, Irene Scarfò<sup>1,2</sup>, Amanda A. Bouffard<sup>1</sup>, Stefanie R. Bailey<sup>1,2</sup>, Praju Vikas Anekal<sup>5</sup>, Paula Montero Llopis<sup>5</sup>, Linda T. Nieman<sup>2</sup>, Yuhui Song<sup>2</sup>, Katherine H. Xu<sup>2</sup>, Trisha R. Berger<sup>1,2</sup>, Michael C. Kann<sup>1,2</sup>, Mark B. Leick<sup>1,2,6</sup>, Harrison Silva<sup>1,2</sup>, Diego Salas-Benito<sup>1,2</sup>, Tamina Kienka<sup>1,2</sup>, Korneel Grauwet<sup>1,2</sup>, Todd D. Armstrong<sup>3,4</sup>, Rui Zhang<sup>3,4</sup>, Qingfeng Zhu<sup>3,4</sup>, Juan Fu<sup>3,4</sup>, Andrea Schmidts<sup>1,2</sup>, Felix Korell<sup>1,2</sup>, Max Jan<sup>1,2,7</sup>, Bryan D. Choi<sup>1,2,8</sup>, Andrew S. Liss<sup>9</sup>, Genevieve M. Boland<sup>2,10</sup>, David T. Ting<sup>2</sup>, Richard A. Burkhardt<sup>3,4</sup>, Russell W. Jenkins<sup>2</sup>, Lei Zheng<sup>3,4</sup>, Elizabeth M. Jaffee<sup>3,4</sup>, Jacquelyn W. Zimmerman<sup>3,4</sup>, Marcela V. Maus<sup>1,2,6</sup>

<sup>1</sup>Cellular Immunotherapy Program, Cancer Center, Massachusetts General Hospital; Harvard Medical School; Boston, MA, USA.

<sup>2</sup>Cancer Center, Massachusetts General Hospital; Harvard Medical School; Boston, MA, USA.

<sup>3</sup>Sidney Kimmel Comprehensive Cancer Center, Johns Hopkins University; Baltimore, MD, USA

<sup>4</sup>Cancer Convergence Institute and Bloomberg Kimmel Institute at Johns Hopkins; University, Baltimore, MD, USA

<sup>5</sup>MicRoN Core, Harvard Medical School; Boston, MA, USA.

\*Corresponding author: Marcela V. Maus, MD PhD, Cellular Immunotherapy and Hematopoietic Cell Transplant and Cellular Therapy Program, Massachusetts General Hospital and Harvard Medical School; 149 13th Street, Room 3.216, Charlestown, MA 02129, mvmaus@mgh.harvard.edu.

†shared first co-authorship

Author contributions

M.W. and M.V.M. conceptualized the project. M.W., F.B., S.G., A.K., J.W.Z., Y.S., A.A.B. and P.V.A. performed the experiments. M.W., F.B., S.G., A.K., J.W.Z., Y.S., R.W.J., and P.V.A. analyzed results. M.W., F.B., and S.G. created the figures. M.W., I.S., R.C.L., S.R.B., R.J., J.W.Z., S.G., E.M.J. and M.V.M. designed the research. M.W., F.B., T.R.B., and M.V.M. wrote the manuscript. All the authors read, edited, and approved the manuscript.

**Conflicts of interest:** M.V.M. is an inventor on patents related to adoptive cell therapies held by Massachusetts General Hospital and the University of Pennsylvania (some licensed to Novartis). M.V.M. holds equity in 2Seventy Bio, TCR2, Century Therapeutics, Genocea, Oncternal, and Neximmune, and has served as a consultant for multiple companies involved in cell therapies. M.V.M. serves on the Board of Directors of 2Seventy Bio. MVM and M.W. have filed patents related to this work. D.T.T. has received consulting fees from ROME Therapeutics, Tekla Capital, Ikena Oncology, Foundation Medicine, Inc., NanoString Technologies, and Pfizer that are not related to this work. D.T.T. is a founder and has equity in ROME Therapeutics, PanTher Therapeutics, and TellBio, Inc., which is not related to this work. D.T.T. receives research support from ACD-Biotechnie, PureTech Health LLC, and Ribon Therapeutics, which was not used in this work. D.T.T.'s interests were reviewed and are managed by Massachusetts General Hospital and Mass General Brigham in accordance with their conflict-of-interest policies. G.M.B. has sponsored research agreements with: Olink Proteomics, Teiko Bio, InterVenn Biosciences, Palleon Pharmaceuticals. GMB served on advisory boards for: Iovance, Merck, Nektar Therapeutics, Novartis, and Ankyra Therapeutics. GMB consults for: Merck, InterVenn Biosciences, and Ankyra Therapeutics. GMB holds equity in Ankyra Therapeutics. R.C.L. has patents owned by MGH related to cellular therapies and has consulted for Syncopation Life Sciences. R.W.J. is a member of the advisory board for and has a financial interest in Xspera Biosciences Inc., a company focused on using *ex vivo* profiling technology to deliver functional, precision immune-oncology solutions for patients, providers, and drug development companies. E.M.J. reports other support from Abmeta, other support from Adventris, personal fees from Achilles, personal fees from DragonFly, personal fees from Parker Institute and CPRIT, personal fees from Surge and HDTbio, grants from Lustgarten, grants from Genentech, personal fees from Mestag, personal fees from Medical Home Group, grants from BMS, and grants from Break Through Cancer outside the submitted work. J.W.Z. has grant funding from Roche/Genentech as part of their imCORE initiative. The other authors declare no competing interests.

<sup>6</sup>Blood and Marrow Transplant Program, Massachusetts General Hospital; Harvard Medical School; Boston, MA, USA.

<sup>7</sup>Department of Pathology, Massachusetts General Hospital and Harvard Medical School; Boston, MA, USA.

<sup>8</sup>Department of Neurosurgery, Massachusetts General Hospital and Harvard Medical School; Boston, MA, USA.

<sup>9</sup>Division of Gastrointestinal and Oncologic Surgery, Massachusetts General Hospital; Harvard Medical School; Boston, MA, USA.

<sup>10</sup>Department of Surgery, Massachusetts General Hospital and Harvard Medical School; Boston, MA, USA.

## Abstract

**Purpose:** Targeting solid tumors with CAR T-cells remains challenging due to heterogeneous target antigen expression, antigen escape, and the immunosuppressive tumor microenvironment (TME). Pancreatic cancer is characterized by a thick stroma generated by cancer-associated fibroblasts (CAFs), which may contribute to the limited efficacy of mesothelin-directed CAR T-cells in early-phase clinical trials. To provide a more favorable TME for CAR T-cells to target pancreatic ductal adenocarcinoma (PDAC), we generated T-cells with an anti-mesothelin CAR and a secreted T-cell-engaging molecule (TEAM) that targets CAFs through fibroblast activation protein (FAP) and engages T-cells through CD3 (termed meso<sup>FAP</sup> CAR-TEAM cells).

**Experimental design:** Using a suite of *in vitro*, *in vivo*, and *ex vivo* patient-derived models containing cancer cells and CAFs, we examined the ability of meso<sup>FAP</sup> CAR-TEAM cells to target PDAC cells and CAFs within the TME. We developed and used patient-derived *ex vivo* models including patient-derived organoids with patient-matched CAFs and patient-derived organotypic tumor spheroids (PDOTS).

**Results:** We demonstrated specific and significant binding of the TEAM to its respective antigens (CD3 and FAP) when released from mesothelin-targeting CAR T cells, leading to T cell activation and cytotoxicity of the target cell. Meso<sup>FAP</sup> CAR-TEAM cells were superior in eliminating PDAC and CAFs compared to T cells engineered to target either antigen alone in our ex-vivo patient-derived models and in mouse models of PDAC with primary or metastatic liver tumors.

**Conclusions:** CAR-TEAM cells enable modification of tumor stroma, leading to increased elimination of PDAC tumors. This approach represents a promising treatment option for pancreatic cancer.

## INTRODUCTION

Pancreatic ductal adenocarcinoma (PDAC) is a devastating disease with a dismal prognosis (1). The current standard of care for metastatic disease consists of chemotherapy combinations such as FOLFIRINOX (fluorouracil, irinotecan, leucovorin, oxaliplatin) or gemcitabine and nab-paclitaxel (2,3). Though immune checkpoint blockade provides a long-lasting clinical benefit in many cancer types, several phase I and II clinical trials in PDAC

showed no advantage to checkpoint blockade, likely due to the lack of an effective T-cell infiltration (4-7).

The tumor microenvironment (TME) of PDAC has an extracellular matrix- (ECM) and collagen-rich stroma, which is mainly generated by cancer-associated fibroblasts (CAFs) that also play a key role in the survival, proliferation, and invasion of cancer cells (8). CAFs are a heterogeneous population, performing various functions in the PDAC TME. Inflammatory CAFs (iCAF) and myofibroblastic CAFs (myCAFs) are considered the main mediators of PDAC progression and drug resistance (9,10). However, Huang et al. have recently reported that antigen-presenting CAFs (apCAFs) evolve from mesothelial cells during the progression of pancreatic cancer and contribute to immune evasion by inducing T regulatory cell (Treg) formation (11). Another way of PDAC promotion through CAFs has been recently described through a Netrin G1-mediated mechanism via the glutamate and glutamine metabolism by Francescone et al (12). Moreover, Krishnamurty et al. and Hingorani et al. reported on a CAF population expressing leucine-rich-repeat-containing protein 15 (LRRC15+) as an important mediator of PDAC tumor progression and suppressor of tumor immunity (13,14). An approach to increase CD8+ effector T cells with the aim to improve checkpoint blockade (ICB) in a preclinical PDAC model has been recently reported using a blocking CD100 (semaphorin 4D) monoclonal antibody (mAb)(15). Mace et al. and Zhang et al. demonstrated through inhibition of IL-6 or Heat shock protein 90 (Hsp90) increased efficacy in preclinical PDAC models when combined with ICB respectively (16,17)

The ECM generated by CAFs forms a physical barrier that reduces drug distribution at the tumor site and supports the survival and migration of cancer cells (18,19). Additionally, CAFs secrete a variety of growth factors, chemokines, and cytokines that support the invasion and proliferation of tumor cells and change the TME into an immunosuppressive 'immune cell milieu', helping to circumvent immune surveillance (10,20).

Fibroblast activation protein (FAP), a membrane-bound serine protease, has been reported as a pan-CAF marker and is expressed on iCAFs and myCAFs (10). FAP is involved in modulation of the ECM and promoting angiogenesis, epithelial to mesenchymal transition (EMT), and secretion of immunosuppressive factors (21). The expression of FAP is restricted in healthy tissue and is detected on activated fibroblasts associated with wound healing and pathological fibrotic conditions of the lung, liver, and heart (22,23). Moderate to high expression of FAP on stromal tissue in PDAC specimens from pancreatic cancer patients has been correlated with worse clinical outcomes (24). Therefore, FAP represents an ideal antigen to target CAFs and disrupt their role in promoting tumor growth.

Chimeric antigen receptor (CAR) T-cell therapy has been a breakthrough treatment in hematological malignancies, but clinically significant outcomes in solid tumors have yet to be realized (25). Mesothelin has been identified as an ideal cell surface target antigen due to its prevalent overexpression in many solid tumors, including PDAC, and its limited presence in normal tissues (26,27). Several anti-mesothelin CAR T-cells have advanced into clinical trials, such as [NCT01897415](#) and [NCT02159716](#) (28,29). While patients were able to tolerate the treatment well, only limited anti-tumor effects have been reported (26).

We hypothesized that a genetically engineered T-cell product could be designed to target both pancreatic cancer cells and the TME. To this end, we developed a bicistronic lentiviral vector encoding an anti-mesothelin CAR and a secreted T-cell engaging molecule (TEAM) that targets FAP on CAFs and CD3 on T-cells. TEAMS are a form of dual-specific T-cell engagers (TCE), conceptually similar to BiTEs<sup>®</sup>. We termed our mesothelin-targeting, FAP TEAM-secreting CAR T-cell product, meso<sup>FAP</sup> CAR-TEAM cells.

One of the challenges in developing CAR T-cells for PDAC is the lack of preclinical models that sufficiently represent the TME. Most preclinical CAR T-cell research is performed with immunodeficient murine models (30) lacking fibroblasts or CAFs as substantial cells of the TME. When human CAFs are added into these models to mimic the stroma-rich TME, the human stromal cells are replaced by endogenous murine stromal cells over 2-4 weeks (31-33). As part of our evaluation of the function of our meso<sup>FAP</sup> CAR-TEAM cells, we generated several new preclinical PDAC models consisting of PDAC cells combined with CAFs. We used patient-derived *ex vivo* models including patient-derived organoids with patient-matched CAFs and patient-derived organotypic tumor spheroids (PDOTS). Using these novel models, we show that FAP TEAM secretion increases the potency and tumor control of mesothelin-targeting CAR T-cells.

## MATERIALS AND METHODS

### Cell lines

CAPAN-2 (Cat# HTB-80, RRID:CVL\_0026), BxPC-3 (Cat# CRL-1687), and ASPC-1 (Cat# CRL-1682, RRID:CVCL\_0152) PDAC cell lines were purchased from American Type Culture Collection (ATCC) and cultured as recommended. An immortalized PDX-derived PDAC cell line, PDX 1294, was a kind gift from the Liss lab at MGH. PDX 1294 was derived from a patient with pancreatic cancer and has recently been classified and analyzed on transcriptional level and been compared to other patient PDAC tumor samples (868 different patients) as well as 111 cell lines and 26 PDX-derived cell lines (34). It contains a Gln61 His mutation in the KRAS gene and shows increased CD274 (PD-L1) mRNA expression level. PDX 1294 was cultured in DMEM:F12 (ATCC) supplemented with 10% FBS and 1% Penicillin/Streptomycin. TrypLE Express (Gibco) was used to disassociate PDAC cell lines between routine passaging to preserve expression of mesothelin. Click beetle green luciferase (CBG) and enhanced green fluorescence protein (eGFP) were transduced into all PDAC cell lines. The cells were sorted on a BD FACSAria to ensure 100% GFP expression. Unless otherwise stated, all mentions of PDAC cell lines refer to their CBG/GFP variant. AsPC-1 mesothelin knock-out overexpressing human FAP cells have been generated as follows. Briefly, AsPC-1 cells have been electroporated with 10ug of Cas9 mRNA and 0.3nmol of sgRNA (Synthego CRISPREvolution GGAGACAGACCAUGUCGACG) using BTX ECM 830 electroporator. Human FAP or murine FAP overexpression was obtained by transducing mesothelin knock-out AsPC-1 with a lentiviral vector encoding for human FAP cDNA (NP\_004451.2) or murine FAP cDNA (NP\_032012.1). Efficient knock-out of mesothelin and FAP expression were measured by flow cytometry and mesothelin knock-out (human or mouse) FAP+ AsPC-1 pure population was isolated by cell sorting.

HFF (Cat# SCRC-1041) and MRC-5 (Cat# CCL-171) fibroblast cell lines were obtained from ATCC and cultured as recommended. MRC-5 and HFF have been transduced with CBG and eGFP as described above. CAF-1 was kindly provided by the Ting lab at MGH, Harvard Medical School. CAF-1 cells were disassociated with 0.25% Trypsin-EDTA (Gibco) for passaging and cultured with DMEM (ATCC) supplemented with 10% FBS and 1% Penicillin/Streptomycin (D10). All cell lines were routinely tested for mycoplasma contamination. Cell lines ordered from ATCC were used within 6 months of ordering or authenticated via STR analysis.

### Generation of CAR constructs

Transgenes for meso<sup>FAP</sup>, CD19<sup>FAP</sup>, and meso<sup>CD19</sup> CAR<sup>TEAM</sup>, anti-FAP, and anti-mesothelin CAR alone were designed in Geneious Prime (Version 2020.05). After synthesizing, the constructs were cloned into a lentiviral plasmid backbone regulated by a human EF-1 $\alpha$  promoter (Genscript). Each CAR construct contains a CD8 hinge and transmembrane domains, a 4-1BB co-stimulatory domain, and an intracellular CD3z signaling domain. Each construct also contains a mCherry as a fluorescent marker for the evaluation of transduction efficiency, as previously described (35-38). TEAM sequences were designed with an IgK leader, scFvs against either FAP or CD19 and human CD3, followed by a linked His-tag (39). The scFvs against mesothelin, FAP, and CD19 were derived from sequences of SS1, sibrotuzumab, and blinatumomab, respectively (available to the public).

### CAR T-cell production

Under an institutional review board (IRB)-exempt protocol, leukapheresis product from anonymous healthy human donors was purchased from the MGH blood bank. T-cell Isolation kits (Stem Cell Technologies) were used according to manufacturer protocols and T-cells were cryopreserved. For CAR-T cell production, cells were thawed in R10 media and activated with human CD3/CD28 Dynabeads (Life Technologies), which were added at a 3:1 bead to T-cell ratio, along with 20 IU/mL media of recombinant human IL-2 (PeproTech). The next day, a corresponding amount of lentivirus was added to each well to have the appropriate MOI per construct. Untransduced T-cells (UTD) from matching donors were cultured simultaneously under the same conditions to serve as controls. Every 2-3 days, media was doubled and IL-2 was added to a final concentration of 20IU/mL. Magnetic separation was used to remove Dynabeads from T-cell culture on Day 7. If needed, 2-3 million total T-cells from each condition were taken for sorting on Day 8 on a BD FACSAria based on mCherry expression through a similar MFI gate across all constructs, to account for differences in surface expression of CAR. Sorted CAR T-cells were kept in culture and expanded as described above every 2-3 days until Day 14-15 and used directly for *in vitro* assays. On Day 14-15, expression of mCherry was measured via flow cytometry to calculate the transduction efficiency. Bulk CAR T-cells were then normalized across constructs and donors to the lowest transduction efficiency prior to cryopreservation or in assays.

### Flow cytometry

The following antibody clones were used for flow cytometry: His-tag (ThermoFisher, HIS.H8), Mesothelin (Maus-Lab antibody, A2A11), Mouse Fab2 (Cell Signaling, 4410), hFAP (R&D, 427819), mFAP (R&D, MAB9727), Rat IgG (ThermoFisher, A48263), CD69

(Biolegend, FN50). For co-culture phenotyping: CD3 (BD, SK7), CD4 (BD, SK3), CD8 (BD, SK1), CCR7 (BD, 150503), CD45RA (Biolegend, HI100), PD-1 (BD, EH12.1), LAG-3 (BD, T47-530), TIM-3 (BD, 7D3). For direct staining of anti-mesothelin ScFv (SS1) expression, we used FITC-Labeled Human Mesothelin (ACROBiosystems, MSN-HF223). For human CAR T quantification in the peripheral blood of NSG mice Trucount tubes (BD Biosciences, 340334) were used according to the manufacturer's protocol. For co-culture sorting: CD3 (BD, SK7) and CD45 (BD, HI30). Appropriate isotype control antibodies were used as necessary. In general, cells were washed in PBS + 2% FBS before staining with respective antibodies at ambient temperature for 15 minutes in the dark. Cells were washed again and stained with DAPI to assess cell viability before analyzing on a BD Fortessa X-20. Analysis was done in FlowJo and SPICE was used to visualize varying expressions of exhaustion markers.

### Luciferase killing assay

CAR T-cells or UTDs were co-incubated with target-cells that express CBG luciferase at varying Effector:Target (E:T) ratios. At indicated time points, cells were lysed with a luciferase assay kit (Promega), and luciferase activity was read on a Biotek Neo2 luminescence plate reader. Specific lysis was calculated with the formula: % specific lysis = ((Luminescence Tumor only) – (Luminescence Tumor + CART)) / (Luminescence Tumor only) x 100%.

### Real-time cytotoxicity assay

Cell impedance cytotoxicity experiments were performed on an xCELLigence real-time cell analysis (RTCA) MP instrument (ACEA Biosciences). Respective target cells were coated on an ACEA plate for about 24 hours before adding T-cells in the indicated E:T ratios, or leaving tumor-only wells. For the inlet experiments, CAFs were first coated on the plate as target cells. Sorted CAR<sup>TEAM</sup> cells were then added to the top of the inlet, while UTD T-cells, for a 1:1 or 1:10 (E:T) ratio were added to the well below the inlet. ASPC-1 experiments used plates coated anti-CD9. Cell index was recorded for each well and specific lysis was calculated by the software provided by the manufacturer.

### Co-culture repeat stimulation assay

On day 0, sorted CAR T-cells were phenotypically analyzed using flow cytometry to acquire their baseline phenotype. A 1:1 ratio of ASPC-1:CAF was added to each well of a 24-well plate and allowed to settle at 37°C for 1-2 hours. MFI-sorted CAR T-cells expressing the same level of mCherry or UTDs were added in biological triplicates per condition into the prepared 24 well plates to have a final ASPC-1:CAF-1:T-cell ratio of 1:1:2. The entire experiment was plated in duplicate so that one set of plates could be used to count CAR T-cell expansion and determine their phenotype while the other set was used to isolate RNA for expression analysis. Every 7 days, the T-cells in one set of plates were gently resuspended and a portion of the cells (at least 1e5) were stained for flow cytometry with a propidium iodide & acridine orange viability stain (Logos Biosystems) and phenotypic markers. The percentage of CAR T-cells was determined by live, CD3+mCherry+ cells, UTDs were identified as CD3+mCherry-, CAF as CD3-mCherry+, and ASPC-1 as GFP+. T-cell expansion was determined by the number of T-cells (calculated based on the total

number of cells and percentage of T-cells determined by flow) compared to the number of T-cells added to the culture on day 0. For subsequent stimulations, the number of CAF and ASPC-1 cells needed to have a 1:1:2 ratio of ASPC-1:CAF-1:T-cell was calculated based on the total number of T-cells per condition and added to new 24 well plates as described for day 0. The cells resuspended for flow from the previous plate were then added to the new plates and incubated for another 7 days. On the same day, the replicate plates for RNA isolation were completely resuspended and the cells were sorted on a BD FACS Aria using DAPI, mCherry, CD3, and CD45 gates to harvest only the CAR T-cells. At least 10,000 cells were sorted out, washed once in PBS, pelleted, and frozen directly at  $-80^{\circ}\text{C}$  for RNA-expression analysis.

### RNA-expression analysis

Frozen sorted CAR T-cell pellets from co-culture experiments using MFI sorted CAR T-cells (expressing the same level of mCherry) or UTDs at various time points (as described above) were directly lysed with RLT buffer (Qiagen) on ice and hybridized to probes from the CAR-T CodeSet and additional probes from a custom CodeSet (Nanostring), as described in manufacturer instructions. All assays were performed on a nCounter MAX Analysis System (Nanostring), while the nSolver and nSolver Advanced Analysis program was used for all analyses.

### Confocal live cell, time-lapse microscopy

CAF and ASPC-1 cells, at ratios of 1:1, were added to Ibidi 8 well glass bottom slides (ibid80826) and incubated overnight at  $37^{\circ}\text{C}$ . Sorted CAR T-cells and UTD T-cells were stained with a Cell Tracker Deep Red kit (Invitrogen, C34565) as per the manufacturer's instructions. The cells were added and allowed to attach and equilibrate for approximately 30 minutes before imaging. Live cell, time-lapse imaging was performed as recently described by Larson et al (38). Time-lapses were acquired every 10 seconds up to 5 minutes. A custom macro was made in FIJI v4 to analyze the cell tracking and can be viewed on GitHub (<https://github.com/prajuvikas/PV-2022May-Edge-dynamics-Analysis.git>). Briefly, the T-cells were background subtracted and smoothed before intensity-based thresholding and size filtering. Given the variation in the microenvironment of the T-cells, we defined regions of interest (ROIs) for specific T-cells in the field of view that either interacted with CAFs and/or cancer cells or neither. The T-cell masks were then analyzed for differences between any 2 adjacent time points as the change in cell area. This change in area was then averaged across 20 time points to give an average change in area for each T-cell.

### Avidity assessment with acoustic force cell microscopy

Poly-L Lysine coated flow cell z-Movi chips (LUMICKS) were seeded with ASPC-1 and CAF cells at a 1:1 ratio, before incubating for 2-3 hours. Sorted CAR T-cells and UTD T-cells were stained with a CellTrace Far red dye kit (Thermo Fisher). Each chip was run with meso<sup>FAP</sup>, meso<sup>CD19</sup>, and UTD T-cells, after a 5-minute binding period, and visualized on the z-Movi cell avidity analyzer (LUMICKS). The order of cells loaded was such that those CAR<sup>TEAM</sup> with a TEAM with predicted specific binding were added later, to prevent confounding of the binding of control cells (such as coating the cell layer with TEAM

thereby providing anti-CD3 domains). The percentage of cells bound as a function of acoustic force applied was then analyzed through Ocean software (LUMICKS).

### **In vivo models**

NOD-SCID- $\gamma$  chain  $-/-$  (NSG) mice (The Jackson Laboratory) were housed and bred at the Massachusetts General Hospital (MGH) Center for Cancer Research under pathogen-free conditions. Mice were maintained and used for conducting experiments in adherence to an MGH Institutional Animal Care and Use Committee (IACUC)-approved protocol (#2020N000114). All mouse handling, including injections and monitoring, was performed by an animal technician who was not made aware of presumed results. Mice were normalized before treatment to have similar tumor engraftment (as measured by mean caliper measurement) across all groups. CAF-1:PDAC was resuspended in 150ul of a 1:1 mixture of PBS and Matrigel (Corning) and injected into each mouse subcutaneously. Caliper measurements were taken biweekly. 2, 7, or 12 days after injection CAR T-cells were thawed, washed twice with PBS, and resuspended to  $3 \times 10^6$  CAR T-cells/100uL PBS and injected intravenously through the tail vein. Mouse experiments continued until IACUC guidelines recommended euthanasia. The liver metastatic model utilized in this study has been previously described and is outlined in more detail in the Supplementary Methods (40,41).

### **Immunohistochemistry**

After mice were euthanized, tumor was extracted and fixed in 4% PFA overnight, washed with PBS, and stored in 70% EtOH until staining. Tissue slides were then made and embedded in paraffin. Slides were stained for CD3, mCherry, GFP, and FAP by the specialized histopathology services core facility at MGH. White balancing correction was performed for all images. For clarity improvement, we applied identical brightness and contrast adjustment. Quantification of the respective stains was done in FIJI, an ImageJ software package, by converting the image to 8-bit and adjusting the threshold to exclude background signal compared to the stain, a protocol described by Yang et al. (42).

### **Multiplex-ISH-IF**

Multiplex-ISH-IF was performed by the specialized imaging facility at MGH and is described in more detail in the Supplementary Methods. Briefly, FFPE tissue sections were stained with a panel of 4 RNA probes (Hs-FAP 411978, GFP 409018, mCherry 431208, Hs-CD3E 553978) and one Mesothelin antibody (Abcam ab236546). Whole slide images were acquired at 20x (0.5um) resolution. Cell segmentation and phenotyping were performed within annotated tumor regions using HALO Image Analysis Platform and HALO AI (Indica Labs). Liver samples were stained at Johns Hopkins Sidney Kimmel Comprehensive Center Tumor Microenvironment Core using a multiplex IHC protocol as previously described and outlined in more detail in the Supplementary Methods (43).

### **Patient-derived organotypic tumor spheroids (PDOTS)**

Tumor samples were collected from patients and analyzed according to Dana-Farber/Harvard Cancer Center IRB-approved protocols. PDOT preparation and analysis are

described in more detail in the Supplementary Methods. Briefly, PDOTS were generated from a fresh tumor specimen. The spheroid-collagen mixture was injected into the center gel region of the 3D microfluidic culture device. Two days later, CAR-T-cells were added to the side/media channel at the desired effector:target (E:T) ratio of 1:3. After an additional three days (Day 5), conditioned media was collected and banked for cytokine profiling. PDOTS were stained and imaged for viability assessment.

### Patient-derived Organoids

Patient-derived organoids (PDOs) and matching CAFs were generated from patient surgical specimens following a combination of mechanical and enzymatic dissociation as recently described (44). CAR-T-cells were combined with PDOs and CAFs at a ratio of 1:3:12 organoids to CAFs to T-cells in 25% Matrigel. Cells were maintained in co-culture for a total of 5 days with an interim harvest on day 2. A more detailed description of PDO generation and analysis is provided in the Supplementary Methods.

### Patient Samples

Written informed consent was obtained from each subject. This study was conducted in accordance with the declaration of Helsinki.

### Statistics

Data is generally depicted as mean  $\pm$  standard error of the mean, unless stated otherwise within figure legends. Statistically significant differences were determined by tests as indicated within figure legends.  $P < 0.05$  was considered as significant. P-values are indicated with asterisks as indicated in each figure legend and listed as follows: \* =  $p < 0.05$ , \*\* =  $p < 0.01$ , \*\*\* =  $p < 0.001$ , \*\*\*\* =  $p < 0.0001$ , and ns =  $p > 0.05$ . The number of repeated biological and technical replicates is indicated in the corresponding figure legends. Statistical analysis was conducted in GraphPad Prism (Version 9.4.1).

### Data Availability Statement

All requests for raw and analyzed data will be reviewed by Massachusetts General Hospital to determine if they are subject to intellectual property or confidentiality obligations. Patient-related data not included in the paper may be subject to patient confidentiality. Any data and materials that can be shared will be released using a material transfer agreement. Please contact Marcela V. Maus at mvmaus@mgh.harvard.edu.

## RESULTS

### Meso<sup>FAP</sup> CAR-TEAM cells lyse mesothelin+ PDAC cells and specifically recognize FAP through the TEAM

We generated a bicistronic lentiviral vector encoding an anti-mesothelin CAR with a secreted T-cell engaging molecule (TEAM) consisting of an anti-FAP domain and an anti-CD3 domain (Figure 1A, B). We named this construct meso<sup>FAP</sup>. As controls, we generated meso<sup>CD19</sup> and CD19<sup>FAP</sup> constructs consisting of an anti-mesothelin CAR with a CD19 TEAM or an anti-CD19 CAR with a FAP TEAM, respectively. We also generated a

headless<sup>FAP</sup> construct consisting of only the intracellular CAR signaling domain and a FAP TEAM (Figure 1B). All constructs were based on the EF1-alpha-driven second-generation anti-mesothelin CAR backbone containing the intracellular domains 4-1BB and CD3z. The TEAM was designed by linking two single-chain variable fragments (scFvs), one binding the target and one binding CD3. A polyhistidine-tag (His-tag) sequence was added to facilitate detection, as we have previously reported (39) (Figure 1B). We achieved sufficient lentiviral-mediated gene transfer of CAR<sup>TEAM</sup> transgenes into primary human T-cells, with a median transduction efficiency of 20.6%, 27.7%, and 49.6% for meso<sup>FAP</sup>, CD19<sup>FAP</sup>, and meso<sup>CD19</sup> respectively (Supplementary Figure S1A). Linear correlation between the expression of fluorescent reporter (mCherry) and the CAR molecule was confirmed by FITC-labelled mesothelin staining (Supplementary Figure S1B).

Mesothelin is highly expressed in 80-85% of PDAC samples (27). We detected mesothelin on a patient-derived xenograft (PDX) cell line (1294) and the established PDAC cell lines AsPC-1, BxPC-3, and CAPAN-2 (Figure 1C; Supplementary Fig S1C). To evaluate CAR T-cell activation and cytotoxicity in response to mesothelin, we measured CD69 expression on CAR T-cells upon interaction with mesothelin-coated plates (Supplementary Figure S1D), and we performed luciferase-based killing assays on CAR T-cells co-cultured with PDAC cell lines (which were previously transduced with luciferase and GFP) or real-time cytotoxicity assays on CAR T-cells co-cultured with PDX cells (Figure 1D, E; Supplementary Figure S1E, F). All CAR T-cells containing the meso-CAR (meso<sup>FAP</sup> and meso<sup>CD19</sup>) significantly upregulated CD69 and lysed PDAC cells upon interaction *in vitro*, whereas untransduced (UTD), CD19<sup>FAP</sup>, or headless<sup>FAP</sup> CAR T-cells did not.

Fibroblast activation protein (FAP) is used to identify cancer-associated fibroblasts (CAFs) (10,45) and activated fibroblasts. Accordingly, we detected FAP on immortalized CAF cells (CAF-1) and the fibroblast lines MRC-5 and HFF (Figure 1F, G; Supplementary Figure S1G). CAF-1 cells are primary PDAC patient-derived cancer-associated fibroblast cells that have been further immortalized and transduced with hTERT and mCherry. CAF-1 cells have recently extensively been characterized by Ligorio et al. (46), demonstrating that CAF-1 cells closely recapitulate the main features of endogenous CAFs. Indeed, CAF-1 cells have been shown to promote PDAC growth and metastasis formation in mouse models of PDAC. In addition, Oh et al. have demonstrated that CAF-1 secrete TGF-beta1, a known suppressor of effector T cells (47). TEAM secretion from CAR-TEAM cells and their ability to bind their target was examined using supernatant from transduced human CAR-TEAM cells mixed with the FAP+ human fibroblast cell line HFF or the CD19-transduced cell line K562. TEAM binding to FAP or CD19 was detected using a secondary anti-His-tag antibody. We detected specific and significant binding of the TEAMS to their respective antigen-expressing cell line (Figure 1 H, I). To test the CD3-binding activity of TEAMS, we incubated UTD T-cells with concentrated supernatant from HEK cells transduced with the headless<sup>FAP</sup> construct. We detected TEAM molecules on the surface of UTDs using flow cytometry for the His-tag (Supplementary Figure S1H). When MRC-5 fibroblasts were treated with meso<sup>FAP</sup>, meso<sup>CD19</sup>, or UTD T-cells and analyzed in a luciferase-based killing assay, only the meso<sup>FAP</sup> T-cells eliminated the FAP-positive target cells, whereas meso<sup>CD19</sup> T-cells or UTDs did not (Figure 1J). Similarly, FAP-specific CAR-TEAM cells eliminated FAP-transduced HEK cells (FAP+ HEKs), whereas untransduced HEK cells or FAP+ HEK

cells treated with UTD were not eliminated (Supplementary Figure S1I). In the absence of FAP, binding of CD3 by TEAMs did not impact the expansion of CAR-TEAM cells compared to UTD (Supplementary Figure S1J).

### **Meso<sup>FAP</sup> CAR-TEAM cells lyse CAFs and outperform control CAR T-cells in co-culture assays combining PDAC and CAFs**

To test whether meso<sup>FAP</sup> CAR-TEAM cells eradicate FAP-expressing fibroblast cell lines, we performed three types of co-culture conditions in real-time cytotoxicity assays. First, we treated HFF cells 1:1 with meso<sup>FAP</sup>, meso<sup>CD19</sup>, or meso CAR-TEAM cells, UTD T-cells alone, or UTDs combined with supernatant from meso<sup>FAP</sup> CAR-TEAM cells (containing FAP-targeting TEAM) and measured cytotoxicity. Only meso<sup>FAP</sup> CAR-TEAM cells and UTDs combined with supernatant containing the anti-FAP TEAM eliminated FAP+ HFF cells (Figure 2A, B).

Second, we wanted to further demonstrate the activity of the TEAM independent of the CAR T-cell, therefore, we examined cytotoxicity using a 0.4mm trans-well system to create a physical barrier between CAR-TEAM cells and UTD T-cells. We plated CAF-1 cells in the lower chamber and allowed them to attach. We then added UTDs to the lower chamber and sorted CAR-TEAM cells to the upper chamber (Figure 2C). UTDs eliminated CAF-1 in the lower compartment when FAP TEAM secreting cells were in the upper chamber (Figure 2D). We noted a 12h delay in CAF-1 killing compared to when meso<sup>FAP</sup> CAR-TEAM cells were in direct contact with FAP+ target cells. We hypothesized this delay was due to the kinetics of diffusion of the TEAM into the lower compartment of the trans-well system (Figure 2C, D).

Third, we evaluated meso<sup>FAP</sup> CAR-TEAM cells in a system containing both PDAC cells and CAFs. We first co-cultured AsPC-1 and CAF-1 with unsorted (containing UTD) CAR-TEAM cells, meso CAR T-cells, or UTDs. We first plated CAFs and PDACs at a 1:1 ratio. We then added unsorted CAR-TEAM cells (containing UTDs) at a ratio of 0.2 T-cell: 1 CAF : 1 PDAC. Meso<sup>FAP</sup> CAR-TEAM cells containing UTDs clearly outperformed meso<sup>CD19</sup> and meso CAR T-cells (Figure 2E, F). Additional ratios of 1 T-cell : 1 CAF : 1 PDAC showed similar results. Increasing the ratio to 1 T-cell : 1 CAF : 1 PDAC still showed significant differences between meso<sup>FAP</sup> and meso CAR and between meso<sup>FAP</sup> and meso<sup>CD19</sup> (Supplementary Figure S2A).

To simulate the ratio of CAFs to tumors in tumor samples, as per the literature (46,48), we increased the CAF:PDAC ratio to 9:1. In this setting, the superior effect of meso<sup>FAP</sup> CAR-TEAM cells was, as expected, more compelling (Supplementary Figure S2B, C). Even though CAF cells appear larger, the distribution of both cell types on the plate appears similar (Supplementary Figure S2D). With the same CAF:PDAC ratio of 9:1 we additionally compared meso<sup>FAP</sup> with CD19<sup>FAP</sup> in another cytotoxicity assay showing superiority of meso<sup>FAP</sup> targeting PDAC cells in this co-culture system (Supplementary Figure S2E). Since meso CAR T-cells and meso<sup>CD19</sup> CAR-TEAM cells demonstrated comparable outcomes, we focused on using the meso<sup>CD19</sup> CAR-TEAM cells as the control for meso<sup>FAP</sup> to better reflect the transduction efficiencies and specificity of the TEAM.

## Meso<sup>FAP</sup> CAR-TEAM cells demonstrate increased proliferation and differential activation in the presence of PDAC and CAFs

To explore the proliferative capacity including gene expression of meso<sup>FAP</sup> CAR-TEAM cells, we repeatedly stimulated sorted CAR-TEAM, normalized to mCherry expression level, or UTD T-cells with target PDAC and CAF cells. Six days after the first stimulation with AsPC-1 and CAF-1, meso<sup>FAP</sup> cells had a higher expansion rate than meso<sup>CD19</sup> CAR-TEAM cells (Figure 3A). After a second stimulation, there was a further expansion of meso<sup>FAP</sup> CAR-TEAM cells, whereas meso<sup>CD19</sup> or CD19<sup>FAP</sup> had reduced expansion. This trend continued following a third stimulation. At day 13, after 2 consecutive stimulations, exhaustion markers (TIM-3, PD-1, and LAG-3) were increased on all CAR-TEAM cells compared to UTD by flow cytometric analysis. There was a trend with lower expression of exhaustion markers on meso<sup>FAP</sup> and CD19<sup>FAP</sup> compared to meso<sup>CD19</sup> (Figure 3B). All CAR-TEAM cells had significantly more effector memory and less naïve and central memory T-cells compared to UTD at day 20; however, there were no significant changes in memory phenotype between meso<sup>FAP</sup>, meso<sup>CD19</sup>, and CD19<sup>FAP</sup> as measured by CCR7 and CD45RA expression (Supplementary Figure S3A).

To determine how repeat stimulation with target cells affected CAR-TEAM cell gene expression, we performed NanoString analysis on meso<sup>FAP</sup> and meso<sup>CD19</sup> CAR-TEAM cells 24 hours after the third stimulation with AsPC-1 and CAF-1 (on day 14). Immediately before the gene expression analysis, CAR-TEAM cells were sorted by flow cytometry to separate them from remaining PDAC and CAF cells (Figure 3C). Transcriptional analysis revealed a specific gene profile for meso<sup>FAP</sup> CAR-TEAM cells in comparison to meso<sup>CD19</sup>. The top 3 differentially expressed genes were upregulation of T-cell receptor alpha variable 35 (TRAV35) and tissue inhibitor matrix metalloproteinase-1 (TIMP1) and downregulation of STAT6 (Figure 3D). Pathway scoring presented robust clustering between meso<sup>FAP</sup> and meso<sup>CD19</sup> (Figure 3E). Meso<sup>FAP</sup> CAR-TEAM cells showed increased gene expression in pathways for TCR signaling, TCR diversity, NKT receptors, and cytotoxicity compared to meso<sup>CD19</sup>. Besides increased pathways for persistence, T-cell migration, and co-stimulatory molecules, T-cell exhaustion and activation markers were elevated in meso<sup>FAP</sup> cells. Cell cycle and metabolism pathways were also increased, whereas apoptosis appeared reduced for meso<sup>FAP</sup> in comparison to meso<sup>CD19</sup>. After 3 consecutive stimulations with CAF and PDAC, there were increased T-cell exhaustion markers in meso<sup>FAP</sup> CAR-TEAM cells in the pathway analysis. Nevertheless, the mRNA profiles of PD-1, TIM-3, and LAG-3 were not significantly different between meso<sup>FAP</sup> and meso<sup>CD19</sup> (Supplementary Figure S3B). We also compared the transcriptional profile of meso<sup>FAP</sup> and meso<sup>CD19</sup> on day 0 (just before co-culture with AsPC-1 and CAF-1 cells) versus day 14 (after 3 stimulations with AsPC-1 and CAF-1) and performed a pathway analysis. The top differential gene expression in meso<sup>CD19</sup> CAR-TEAM cells was the downregulation of mitogen-activated protein kinase (MAPK3), whereas meso<sup>FAP</sup> showed highly upregulated IL1A (Supplementary Figure S3C, D). During pathway analysis, both CAR-TEAM cells clustered according to the time point they were collected. The main differences between time points were in TGF-beta signaling, MHC class II antigen presentation, and interferon signaling pathways (Supplementary Figure S3E, F). These signaling pathways were elevated on day 0 in meso<sup>FAP</sup> CAR-TEAM cells compared to day 14, whereas the opposite was true for meso<sup>CD19</sup>. Taken together, these

changes could reflect the signaling that is associated with the CD3 clustering through FAP TEAM after the third stimulation with PDAC and CAFs.

### **Live cell, time-lapse microscopy, and acoustic force microscopy reveal reduced edge dynamics and increased binding avidity of meso<sup>FAP</sup> CAR-TEAM cells**

In comparison to the formation of the immunological synapse on T-cells, little is known about the interactions of CAR T-cells with their target cells. Recently, Larson et al. described the interaction of CAR T-cells with solid tumor cells using live cell, time-lapse microscopy (38). We used this same method to investigate the binding properties between CAR-TEAM cells and target cells. For this purpose, we co-cultured AsPC-1 cells and CAFs in a 1:1 ratio, so that each well contained areas of PDAC and CAF, PDAC alone, or CAFs alone to analyze the interactions of CAR-TEAM cells with each target cell type (Figure 4A). We used percent change in CAR-TEAM cell area over time relative to its initial area (termed 'edge dynamics') as a measure of CAR T-cell movement during these interactions. The edge dynamics of meso<sup>FAP</sup> CAR-TEAM cells were significantly reduced when interacting with PDAC and CAF compared to PDAC alone. However, the difference between meso<sup>FAP</sup> interaction with PDAC and CAF versus CAF alone was not significant (Figure 4A-C; Supplementary Figure S4A; Supplementary Videos S1-4). When meso<sup>FAP</sup> CAR-TEAM cells had no interaction with any target, their edge dynamics increased significantly, suggesting greater mobility of cells searching for their target. We also found a significant reduction in the edge dynamics of meso<sup>CD19</sup> when interacting with PDAC or PDAC and CAF in comparison to meso<sup>CD19</sup> with no target interaction (Figure 4D, E; Supplementary Figure S4B; Supplementary Videos S5-8). UTDs served as a control and showed no significant difference between PDAC and CAF, PDAC alone, CAF alone, or no target (Figure 4F, G; Supplementary Figure S4C; Supplementary Videos S9-12).

We hypothesized that the reduced edge dynamics were due to higher avidity of CAR-TEAM cells when both antigens were encountered. To delineate binding of the TEAM to its ligands (CD3 and target antigen), we used dynamic acoustic force microscopy to measure binding avidity (Figure 4H-J), a method recently described by Larson et al. and Leick et al. (37,38). We coated flow chambers with AsPC-1 and CAF-1 cells at a 1:1 ratio (Supplementary Figure S4D), added CAR-TEAM cells, and exposed them to gradually increasing acoustic force. We found that meso<sup>FAP</sup> CAR-TEAM cells had significantly higher binding avidity in presence of PDAC and CAF compared to meso<sup>CD19</sup> or UTD (Figure 4K). To assess the effect of the FAP TEAM, we compared meso<sup>FAP</sup>, UTD with FAP TEAM added, and meso<sup>CD19</sup> on a flow chamber coated with FAP+ HFF fibroblasts. The binding avidity of meso<sup>FAP</sup> was similar to UTDs combined with FAP TEAM in the presence of FAP+ HFF cells (Figure 4L).

### **Meso<sup>FAP</sup> CAR-TEAM cells are efficacious against PDAC and CAFs in an in vivo model**

To assess the anti-tumor effects of meso<sup>FAP</sup> CAR-TEAM cells *in vivo*, CAF-1 and AsPC-1 cells were subcutaneously injected into the flank of NOD-SCID-II2rg<sup>-/-</sup> (NSG) mice at a 9:1 ratio 2 days prior to treatment with an intravenous injection of CAR-TEAM cells (Figure 5A). Mice treated with meso<sup>FAP</sup> had a significantly reduced tumor burden within the first 10 days compared to mice treated with meso<sup>CD19</sup> or UTD cells. The effect on tumor mass of

meso<sup>CD19</sup> in comparison to UTD was delayed and started to be significant on day 13 (Figure 5B). However, by day 17, the mean tumor volume of meso<sup>CD19</sup>-treated mice had decreased and was no longer significantly different from the meso<sup>FAP</sup>-treated mice. We hypothesized that this decrease might be due to the lack of CAF expansion and functional persistence *in vivo*. When stained for PDAC and T-cells by immunohistochemistry (IHC), tumors from CAR-TEAM-treated mice had significantly reduced AsPC-1 cells and increased CD3+ T-cells compared to UTD (Figure 5C, D).

We next investigated the composition of subcutaneous mixed PDAC/CAF tumors at different time points using multiplex immunofluorescent (IF) RNA-in situ hybridization (ISH) imaging. To detect AsPC-1 cells via IF imaging, we used an anti-mesothelin antibody. Since we had used GFP to detect AsPC-1 cells via IHC, we performed a side-by-side analysis on day 13 tumor tissue. Mesothelin IF and GFP IHC were co-localized in AsPC-1 cells (Supplementary Figure S5A). Before CAR-TEAM cell injection on day 0, the tumors had a homogeneous distribution of mCherry<sup>+</sup>FAP<sup>+</sup> CAFs by multiplex RNA-ISH IF, with interspersed islands of mesothelin<sup>+</sup> PDAC tumor cells (Supplementary Figure S5B). Six days after CAR-TEAM or UTD cell intravenous injection, there was a significant reduction in the number of CAFs (mCherry<sup>+</sup>FAP<sup>+</sup>) and PDAC cells (mesothelin<sup>+</sup>) in mice treated with meso<sup>FAP</sup> compared to mice treated with meso<sup>CD19</sup> or UTD (Supplementary Figure S5C-F). However, the ratios of CAFs, PDAC cells, T-cells (CD3<sup>+</sup>), or CAR T-cells (CD3<sup>+</sup>mCherry<sup>+</sup>) to the total number of cells per quantified tumor area were not significantly different in mice treated with meso<sup>FAP</sup> versus meso<sup>CD19</sup> or UTD on day 8 (Supplementary Figure S5G). We hypothesized that though the tumor size is decreasing the proportion of PDAC, CAF, and T-cells remains the same. Whereas meso<sup>FAP</sup>-treated mice showed a homogenous distribution of CAR-TEAM cells throughout the tumor, we detected regions of meso<sup>CD19</sup>-treated tumors that were not populated by CAR-TEAM cells and were instead populated by CAFs (Supplementary Figure S5C-G).

On day 13 following CAR T-cell treatment, the number of mesothelin-expressing cells was significantly reduced in mice treated with CAR-TEAM cells compared to UTD (Supplementary Figure S5H, I). Moreover, labeling mesothelin, CD3, mCherry, and FAP allowed to distinguish between AsPC-1, CAF-1, and CAR-TEAM including UTD and to exclude trogocytosis on to CAR TEAM (Supplementary Figure S6A). Similar to the IHC results, there was no longer a significant difference in the number of FAP<sup>+</sup> cells in tumors from mice treated with meso<sup>FAP</sup> versus meso<sup>CD19</sup> at day 13, despite meso<sup>FAP</sup> tumors having significantly fewer CAFs on day 6. To determine if this difference was due to the lack of expansion of CAF-1 cells *in vivo*, as observed in previous studies (49), we compared tumor volume and composition when PDAC cells alone, PDAC and CAF cells, or CAF cells alone were injected into NSG mice. We confirmed that CAF-1 cells do not expand when injected subcutaneously with AsPC-1 or PDX1294 cells or when injected alone (Supplementary Figure S6B-E). Therefore, *in vivo* analysis of CAF-1 cells after treatment with meso<sup>FAP</sup> or meso<sup>CD19</sup> is not an accurate depiction of CAF depletion when analyzed longer than one week. The maximal reduction of tumor volume (consisting of PDAC and CAF) after treatment with meso<sup>FAP</sup> compared with meso<sup>CD19</sup> CAR-TEAM cells was reached after 10-13 days, corresponding to the percentage reduction of CAFs over time. We hypothesize that the missing expansion of CAFs when co-injected with AsPC-1 or PDX1294 cells would

explain the limited difference in tumor volume of mice treated with meso<sup>FAP</sup> compared with meso<sup>CD19</sup> at later time points.

In a phase I clinical study of lentiviral transduced anti-mesothelin CAR T-cells targeting solid cancer types, peak copy numbers of CAR T-cells in the peripheral blood were detected between days 6 to 14. The persistence of CAR T did not last longer than 28 days in most of the patients (28). A more recent first-in-human phase I trial with regionally applied anti-mesothelin CAR T-cells in mesothelioma patients demonstrated only 39% of patients with CAR T-cells detectable in the peripheral blood after 100 days (50). Despite normalizing for transduction efficiencies across the different CAR T constructs (Supplementary Figure S7A), we could not detect CAR T-cells in the peripheral blood of mice, engrafted with CAF:AsPC-1 subcutaneous tumors, treated with intravenous CAR T-cells. While we observed infiltration of CAR T-cells, in the tumor (Figure 5C), we could detect a very low number of CAR T-cells in the peripheral blood (Supplementary Figure S7B) of the same treated mice, suggesting that CAR-TEAM cells mainly traffic and reside at the tumor site making it difficult to infer CAR-T cell persistence from peripheral blood count, at least in NSG mice.

### **Meso<sup>FAP</sup> CAR-TEAM cell treatment is efficacious against a pancreatic tumor mouse model of liver metastasis**

To overcome the limited in vivo persistence of CAFs and assess long-term in vivo effects of meso<sup>FAP</sup> CAR-TEAM, we developed a subcutaneous tumor model consisting of a mixed population of mesothelin-expressing tumor cells (AsPC-1 wt) and FAP-expressing tumor cells (AsPC-1 FAP+ mesothelin  $-/-$ ) (Supplementary Figure S7C). Tumor cells were injected at a 1:1 ratio 7 days prior to treatment with an intravenous dose of CAR-TEAM cells. In this experimental set-up, we observed an initial tumor reduction in mice treated with meso<sup>FAP</sup> and meso<sup>CD19</sup>, consistent with anti-mesothelin CAR activity. Compared to meso<sup>CD19</sup> treated mice, meso<sup>FAP</sup> treated mice were able to completely control tumor growth starting from day 14 and outperformed meso<sup>CD19</sup> over time (Figure 5E, F).

To better understand how CAR-TEAMS performed relative to separate CARs targeting mesothelin and FAP, we leveraged our AsPC-1 wt : AsPC-1 FAP+ meso  $-/-$  mixed model in vivo. For this experiment, we generated a FAP-targeting CAR based on the same scFv as our TEAM (sibrotuzumab) and confirmed its specificity against human (without cross-reactivity to murine) FAP (Supplementary Figure S7D, E, respectively). We then compared mice treated with meso<sup>FAP</sup> to mice treated with anti-meso, anti-FAP, or a 1:1 mix of anti-meso CAR-T cells and anti-FAP CAR-T cells (Supplementary Figure S7F). To further challenge the therapeutic potential of our CAR-T cells, we injected AsPC-1 wt and AsPC-1 FAP+ mesothelin  $-/-$  12 days prior to CAR-T cell treatment to have a higher tumor burden. While all CAR-T cell treatment groups showed some tumor reduction compared to UTDs, only meso<sup>FAP</sup> treated mice showed a significantly reduced tumor burden starting from day 10 (Supplementary Figure S7G). Interestingly, co-injection of FAP and meso CAR T-cells also reduced tumor burden, but only at day 14 and to a lower extent compared than meso<sup>FAP</sup> (Supplementary Figure S7G). These data suggest that meso<sup>FAP</sup> exhibits in vivo activity

against both mesothelin and FAP-expressing cells comparable to, if not superior than, co-injection of meso and FAP single-targeting CAR-T cells.

Approximately 50% of PDAC patients display metastatic disease at the time of diagnosis, most frequently involving the liver (51). Importantly, FAP+ fibroblasts are abundant within PDAC liver metastases (52), which we also demonstrate (Supplementary Figure S7H, I). Assessing the efficacy of meso<sup>FAP</sup> in a metastatic model of PDAC would lay the foundation for clinical translation. Therefore, we decided to investigate the efficacy of meso<sup>FAP</sup> in an orthotopic model of PDAC liver metastases. We injected ASPC-1 and CAF-1 into the spleens of NSG mice until the formation of liver metastases could be observed, 2 weeks later (Figure 5G). These mice developed liver metastases characterized by a core of tumor cells surrounded by layers of fibroblasts (Figure 5H), reminiscent of the desmoplastic stroma of human PDAC liver metastases (Supplementary Figure S7H, I) (52). Intravenous injection of either meso<sup>FAP</sup> or meso<sup>CD19</sup> resulted in prolonged survival compared to UTDs (Figure 5I). However, only meso<sup>FAP</sup> treatment induced complete clearance of CAF-1 cells in the liver metastases, as shown by immunohistochemistry (IHC) analysis (Figure 5J, K). Collectively, these data suggest that meso<sup>FAP</sup> CAR-T cells control both primary PDAC tumors and liver metastases.

### **Meso<sup>FAP</sup> CAR T-cells decrease tumor growth in an in-vivo PDX-CAF model and are superior in an ex-vivo patient-derived PDAC model of tumor spheroids (PDOTS)**

To assess the efficacy of meso<sup>FAP</sup> in a patient-derived xenograft (PDX) model of PDAC, we co-injected CAFs mixed with PDX1294 cells at a 9:1 ratio into the flank of NSG mice and injected CAR-TEAM cells intravenously two days later (Figure 6A, B). Since CAF-1 cells do not expand *in vivo*, we chose to treat with CAR-TEAM at the same time point after tumor engraftment as for AsPC-1, to recapitulate that PDAC tumors contain a multitude of CAFs. Animals receiving meso<sup>FAP</sup> CAR-TEAM cells had a significant reduction of tumor volume within the first 12 days compared to mice treated with meso<sup>CD19</sup> (Figure 6C). To assess the tumor composition and infiltration of CAR-TEAM cells following treatment, we performed IHC on tumor tissues collected from mice on day 12 after CAR-TEAM treatment. Meso<sup>FAP</sup> treatment significantly reduced GFP+ PDX 1294 cells compared to the meso<sup>CD19</sup>, UTD, and tumor-only groups. In addition, meso<sup>FAP</sup> significantly reduced the amount of FAP+ CAF-1 compared to meso<sup>CD19</sup> or UTD cells, which were not significantly different from each other (Figure 6D, E).

To investigate the effects of CAR-TEAM cells in a patient-derived PDAC model containing autologous tumor and immune/stromal cells, we analyzed the efficacy of meso<sup>FAP</sup>, meso<sup>CD19</sup>, CD19<sup>FAP</sup> using patient-derived organotypic tumor spheroids (PDOTS) (53) from a patient with locally advanced PDAC. PDOTS containing CAFs and tumor cells directly from the tumor digest were prepared in collagen hydrogels and injected into the center gel region of a 3D microfluidic culture device. CAR-T cells were loaded into the side channels via the media port (Figure 6F). After 5 days, meso<sup>FAP</sup>-treated PDOTS significantly reduced the percent of tumor cell area with a corresponding increase in dead cells compared to meso<sup>CD19</sup>-treated PDOTS (Figure 6G). This effect was more pronounced when meso<sup>FAP</sup> treatment was compared to CD19<sup>FAP</sup> and UTD. To assess CAR-TEAM cell effector function

in this model, a bead-based immunoassay was used to profile secreted cytokines and chemokines in supernatant harvested from PDOTS on day 5. There was an increase in IFN- $\gamma$ , CXCL-10 (interferon-gamma induced protein = IP-10), GM-CSF, IL-13, and TNF $\alpha$  secretion in meso<sup>FAP</sup>-treated PDOTS compared to meso<sup>CD19</sup>-treated PDOTS (Figure 6H).

### **Meso<sup>FAP</sup> CAR-TEAM cells proliferate more and control tumor growth better than control T-cells in a co-culture system of patient-derived organoids with matching CAFs**

Due to the limitations of preclinical human PDAC *in vivo* model systems, such as the lack of matching CAF expansion, we sought to determine the efficacy of meso<sup>FAP</sup> in a patient-derived organoid (PDO) system with matched patient-derived CAFs. To model PDAC and include its stromal-rich TME, PDOs, and CAFs were generated from fresh tumor specimens obtained from 3 different patients undergoing surgical resection (Figure 7A, B). PDOs were screened for mesothelin expression by flow cytometry and CAFs for FAP expression by western blot (Supplementary Figure S8A-E). CAR-TEAM or UTD were added to the co-cultures in 25% Matrigel domes and profiled on day 2 and day 5. After 5 days, there was a substantial change in the structural organization of meso<sup>FAP</sup>-treated co-cultures compared to meso<sup>CD19</sup> and UTD by transillumination microscopy. Whereas the organoid co-cultures treated with meso<sup>CD19</sup> and UTD were still densely organized, meso<sup>FAP</sup>-treated co-cultures were disintegrated, rounded up, and appeared to have lost their structure due to the effective T-cell killing (Figure 7C). Cell recovery from the organoid co-cultures on day 5 revealed a significant expansion of CD3+ cells in meso<sup>FAP</sup>-treated co-cultures compared to meso<sup>CD19</sup> (Figure 7D; Supplementary Figure S8F-H), supporting our previous *in vitro* findings. Flow cytometric analysis of the components of the organoid co-culture system showed a significant reduction of mesothelin-expressing PDO cells on day 5 with meso<sup>FAP</sup> and meso<sup>CD19</sup> CAR-TEAM cell treatment compared to UTD (Figure 7E, F). We also detected a significant reduction in CAFs at days 2 and 5 in organoid co-cultures treated with meso<sup>FAP</sup> compared to meso<sup>CD19</sup> or UTD, suggesting superior CAF targeting by meso<sup>FAP</sup> CAR-TEAM (Figure 7E, G). Analysis of activation or exhaustion markers on the T-cells revealed a higher percentage of CD69+, LAG-3+, PD-1+, and TIM-3+ cells in the organoid system treated with meso<sup>FAP</sup> compared to meso<sup>CD19</sup> and UTD on day 2 and day 5 after treatment (Figure 7H; Supplementary Figure S8I-K). In our data, organoids were cultured in CAF-conditioned media for 3 days (Supplementary Figure S8L) and then we used flow cytometry to obtain live cells (Supplementary Figure S8M) and measure proliferation by Ki-67 (Supplementary Figure S8N). We see a tremendous increase in proliferation in this set of conditions, suggesting the CAFs are secreting factors that are promoting organoid proliferation; the factors secreted by CAFs can be used to replace the robust growth factor support initially described by Tuveson and colleagues (44). In the first PDO VITAL assay of its kind, we detect cytotoxicity of CAR T-cells towards PDOs after 48 hours and demonstrate a trend toward the superior killing of PDO by meso<sup>FAP</sup> compared to meso<sup>CD19</sup>. Since there were several rounds of adaptations and technical challenges of this novel assay, technical duplicates are reported (Figure 7I).

Altogether these data reveal that a novel CAR T-cell secreting a TEAM that targets CAFs in the TME is superior in terms of proliferation, persistence, and tumor eradication compared to CAR T-cells targeting mesothelin alone. Moreover, we show that meso<sup>FAP</sup>

are differentially activated in model systems containing PDAC and CAFs. Finally, we demonstrate that PDOTS and organoids provide a feasible platform for the analysis of CAR T-cells in a multidimensional environment that represents PDAC and its TME.

## DISCUSSION

Targeting solid tumors remains a hurdle for CAR T-cell applications due to limitations in suitable target antigens, tumor antigen escape, and the immunosuppressive TME which can limit T-cell infiltration and sustained function (25,30). Pancreatic cancer is known for its dense stroma derived from CAFs, which is a critical factor in the TME. The immunosuppressive effects of FAP-expressing CAFs in PDAC have been reported by Kraman et al. (54). In this context, the chemokine axis comprised of CXC-chemokine ligand 12 (CXCL12) and its receptor CXC-chemokine receptor 4 (CXCR4) has been described to inhibit T cell infiltration and support tumor growth in the KPC PDAC mouse model (55). Data from patients with colorectal cancer also suggest that FAP-expressing CAFs correlated with dense immunosuppressive macrophage-rich stroma and reduced response to immunotherapy (56).

We have previously shown that CAR T-cells secreting T-cell engagers (TCE) can be used to bypass antigen escape in glioblastoma (39). Therefore, we undertook a similar technological approach but engineered the TCE to target the TME to specifically overcome a critical barrier in pancreatic cancer. In the current study, we introduce meso<sup>FAP</sup> CAR-TEAM cells that target two antigens, mesothelin, and FAP, thereby eliminating the two predominant cell types in pancreatic cancer, PDAC and CAFs, as shown in different preclinical models. Preclinical models that represent the TME have been inadequate for various reasons, such as pre-clinical studies of human CAR T-cells being performed in immunodeficient murine models, which cannot endogenously form the human TME. These animals lack human myeloid cells and human stroma (fibroblasts or CAFs), which are necessary components to investigate the TME (57,58). One strength of our work lies in the multi-dimensional analysis of meso<sup>FAP</sup> CAR-TEAM cells across different preclinical models of pancreatic cancer combining PDAC and CAFs *in vitro*, *in vivo*, and in patient-derived *ex vivo* models such as patient-derived organoids with patient-matched CAFs and patient-derived tumor spheroids (PDOTS) containing autologous tumor and immune/stromal cells (59). Recently, Lee et al. presented a preclinical non-invasive PET-based (positron emission tomography) approach to monitor and predict anti-FAP CAR T-cell responses *in vitro* and *in vivo* using a radiolabeled FAP inhibitor in an NSG mouse lung cancer model (31). In contrast to our work, the authors used a cross-species anti-FAP CAR targeting murine and human FAP. The FAP-directed antibody that we used to derive our FAP-TEAM was human-specific and did not cross-react with murine FAP (23). Indeed, there is more than one approach that aims to target CAFs in the stroma. A recent manuscript using a syngeneic PDAC model reported about increased efficacy of sequential application of anti-FAP CARs combined with anti-claudin18.2 CARs (60). A recently published manuscript (bioRxiv 2023:2023.04.13.536777) demonstrates the use of anti-FAP CARs combined with anti-mesothelin CARs in syngeneic tumor models and in a xenograft model. This approach may also be feasible, yet does not negate the value of the approach we have taken; requiring two CARs and two vectors may increase the cost of

translation and release testing of two “drug products,” so there may be advantages to the approach we have explored.

Although we could not test meso<sup>FAP</sup> CAR-TEAM cells in a syngeneic murine PDAC model, due to cross-species immune barriers, we used an *in vivo* model combining human CAFs with human PDAC cells in NSG mice. This is analogous to the work of Sakemura et al., who recently reported on the effect of anti-BCMA and anti-FAP CAR T-cells in an NSG model engrafted with multiple myeloma tumor cell lines and bone marrow-derived CAFs (61). Although syngeneic tumor models allow for better mechanistic understanding of the biology and cellular interactions, it can be difficult to balance the interpretation of mechanistic studies that use murine reagents relative to the behavior of the human reagents in various humanized models. Here, we prioritized testing in various human-based models, including organoids, PDOTS, and hemi-splenectomy models, in part because we did not have access to critical reagents needed to test this concept in murine form.

There is growing interest in PDOs as they recapitulate not only the phenotype but also the molecular characteristics of the primary tumor. Seppälä et al. recently reported on the prediction of clinical response to chemotherapy in PDAC patients based on pharmacotyping of PDOs (62). To analyze and design interactions and function of PDOs with cellular immunotherapies, Dekkers et al. recently reported on a novel technology combining single-cell 3D imaging with transcriptomic profiling of engineered T-cells with PDOs (63). Finally, we show in our work the superiority of meso<sup>FAP</sup> CAR T-cells in comparison to control constructs using co-culture transillumination imaging and flow cytometry for the analysis of CAR-TEAM-treated PDOs from PDAC patients combined with matching CAFs. PDOTS, as another patient-derived *ex-vivo* system, combines PDAC and features of the TME (53). Though PDOTS have not yet been used to predict clinical responses, they have been used to examine CAR NK cells in combination with STING agonists to demonstrate efficacy against malignant pleural mesothelioma (59). Using PDOTS as a representative *ex-vivo* system, we demonstrate that meso<sup>FAP</sup> CAR-TEAM cells are a promising therapeutic candidate in pancreatic tumors.

Consistent with our previous work (39), we found that secretion of the TEAM conferred unexpected benefits to the phenotype and function of the transduced T-cells. CAR T-cells are known to enter a dysfunctional state that limits their efficacy upon reaching the immunosuppressive TME (25,64). We found that when we repeatedly stimulated CAR-TEAM cells with PDAC and CAF cells *in vitro*, meso<sup>FAP</sup> CAR-TEAM cells had a significant proliferation advantage compared to control CAR-TEAM cells. We have recently shown that disruption of the IFN $\gamma$ R1 pathway in solid tumors led to reduced avidity and duration of binding between them, and made solid tumor cells more resistant to CAR T-cell killing (38). We also showed that enhanced avidity was associated with increased CAR T-cell expansion and anti-tumor activity *in vivo* in acute myeloid leukemia and multiple myeloma (37). Interestingly, we found here that meso<sup>FAP</sup> CAR-TEAM cells interacting with PDAC and CAFs also had increased avidity, suggesting a potential role for autocrine-bound TEAM molecules in enhancing binding and CAR T-cell killing. We note that the increased binding activity could be due to increased adhesion of the TEAM, which could potentially

be achieved independently of CD3 signaling. We hypothesized that these properties could provide an advantage when meso<sup>FAP</sup> CAR T-cells enter the TME of PDAC.

A limitation of our study is the current limited knowledge of the role of FAP+ CAFs in metastatic PDAC. It has been reported by Cohen et al. and Bughda et al. that increased FAP expression on 'tumor-associated myofibroblasts' such as CAFs could be correlated to higher PDAC detection in lymph nodes of PDAC patients (65,66). More recently, a population of mesenchymal stromal cells (MSC) expressing FAP from resected PDAC samples have been associated with tumor promotion, invasion, and formation of metastasis (14,67). Good et al. reported that continuous antigen exposure of anti-mesothelin CAR T-cells within pancreatic cancer leads to a transition from CD8+ CAR T-cell state into a dysfunctional NK-like CAR T-cell state (68). After another stimulation with both antigens such as PDAC and CAFs, we detected an increase of NKT receptor pathways, Treg, and Th17 pathways in meso<sup>FAP</sup> in comparison to meso<sup>CD19</sup>. In contrast to Good et al., we detected increased proliferation and found increased pathways for cytotoxicity in meso<sup>FAP</sup> CAR-TEAM cells compared to meso<sup>CD19</sup> CAR-TEAM cells. We hypothesized that this additional benefit might be accomplished through FAP TEAM, as we also detected an increase of pathways involved in persistence, TCR diversity and TCR signaling, T-cell migration, cell cycle, and costimulatory molecules in meso<sup>FAP</sup> in comparison to meso<sup>CD19</sup>. In line with this observation, we also detected a reduction of TGF-beta and apoptosis pathways.

Clinical trials of anti-mesothelin CAR T-cells for solid tumors, including PDAC, began over a decade ago and suggested that additional functionalities would be required for effective clinical use (69). Unfortunately, repeated infusions of the first-in-human anti-mesothelin CAR T-cell trial ([NCT01355965](#)) led to immunization and sensitization to the CAR itself, and one patient experienced anaphylaxis and cardiac arrest after the third infusion of CAR T-cells (70,71). A follow-on clinical trial ([NCT02159716](#)) used the same CAR construct, now with lentiviral transduced autologous T-cells, and demonstrated a good safety profile with one dose-limiting toxicity (sepsis) treated in the arm without cyclophosphamide. However, anti-tumor responses were limited (28,69). A recent phase 1 clinical trial ([NCT02414269](#)) has shown that local delivery of anti-mesothelin CAR T-cells followed by infusion of the anti-PD1 monoclonal antibody, pembrolizumab, was safe and led to modest antitumor effects in malignant pleural mesothelioma (50). Altogether, these early clinical data indicate that targeting mesothelin with CAR T-cells has acceptable toxicity but modest clinical benefit.

One of the first reports of targeting murine FAP with CAR T-cells in the pre-clinical setting raised safety concerns due to FAP expression in bone marrow stromal cells (BMSC) in mice (23). Wang et al., Kakarla et al., and Lo et al., on the other hand, did not observe severe toxicities when using murine anti-FAP CAR T-cells (72-74). In published syngeneic murine animal models, anti-murine FAP CAR T-cells against cardiac fibrosis were extensively analyzed in a variety of histological tissue sections (s.a. spleen, skin, testis, lungs, intestines, and liver - (22)) and did not indicate toxicities. One limitation of our models is that we could not definitively prove the safety or potential on-target, off-tumor toxicities of secreted or T-cell-bound anti-FAP TEAMS because the anti-FAP sequence used in this manuscript is human-specific and does not cross-react with murine FAP. However, the first clinical

trial investigating sibtrotuzumab was safe and well-tolerated (75). In addition, there are two ongoing trials of FAP-targeting CARs, though the origin of the binder domain is not clear: one phase 1 trial investigating FAP CAR T-cells in 4 patients with malignant pleural mesothelioma (NCT 01722149) demonstrated the persistence of intra-pleural administered anti-FAP-CAR T-cells in peripheral blood without any evidence of on-target off-tumor toxicity (76). Another trial using a fourth-generation anti-Nectin4/FAP CAR T-cell is currently recruiting patients with advanced malignant solid tumors (NCT 03932565). A FAP/4-1BB targeting bispecific fusion protein was recently tested in a phase 1 clinical trial and demonstrated a tolerable safety profile in patients with advanced solid tumors (77). Together these data suggest that targeting FAP with CARs or TEAMS appears safe. Furthermore, mesothelin can also be highly expressed on fibroblasts in damaged liver and has been associated with liver, lung, and kidney fibrosis (78). In such a scenario, it is possible that co-targeting of mesothelin and FAP, whether by dual CARs or a CAR-TEAM approach, could potentially exacerbate off-tumor toxicities; ultimately, many of these questions are only settled with clinical experience.

The advantage of meso<sup>FAP</sup> remains in the generation and secretion of FAP-specific TEAMS at the mesothelin overexpressing tumor site where meso<sup>FAP</sup> accumulate and exert its optimal effects. This would be beneficial compared to peripherally infused TCEs due to their short half-life in blood due to rapid renal clearance. In summary, our work suggests a novel CAR T-cell approach for pancreatic cancer. We demonstrate that meso<sup>FAP</sup> CAR-TEAM cells are not only activated in a different fashion but are also superior in the elimination of PDAC and CAFs in a series of pre-clinical models. Moreover, we show that *ex-vivo* patient-derived samples such as PDO with matching CAFs and PDOTS represent a novel and feasible readout for CAR-TEAM function and analysis.

## Supplementary Material

Refer to Web version on PubMed Central for supplementary material.

## ACKNOWLEDGEMENTS

We thank the core facilities at the MGH Cancer Center: Flow Cytometry, Histopathology, and Blood Bank. Moreover, we thank the multiplex-ISH IHC facility at MGH Cancer Center: Linda Nieman: Individual Contributions to Project; Staining panel development and staining of final slides: Katherine H. Xu, Evan R. Lang, Yuhui Song, Linda T. Nieman; Imaging: Yuhui Song (GFP), Linda T. Nieman (FL); Analysis: Linda T. Nieman, Katherine H. Xu, Yuhui Song. We also thank Ada Tam and Nicholas Ionta in the Sidney Kimmel Comprehensive Cancer Center High Parameter Flow Core which was used for cellular sorting and the Cell Imaging Facility of Sidney Kimmel Comprehensive Cancer Center at Johns Hopkins University, which was used for imaging western blots. Johns Hopkins Sidney Kimmel Comprehensive Cancer Center TME Core and Oncology Tissue Services.

## Funding:

M.W. was supported by the Swiss National Science Foundation (SNSF), Postdoc.Mobility fellowship (P400PM\_186739, M.W.). S.G. was funded in part by NIH/NCI 2T32AI007247-39. F.B. was supported by the American-Italian Cancer Foundation (AICF) and the Italian Foundation for Cancer Research (AIRC). R.C.L. was supported by NIH T32 AI007529. D.S.B. was supported by SEOM (Spanish Society of Medical Oncology, grant for two years in foreign country 2021) and CRIS Foundation Out-Back Programme 2021 Grant (outback2021\_6). A.S. was supported by a John Hansen Research Grant from DKMS (no. DKMS-SLS-JHRG-2020-04). D.T.T. was supported by U01CA228963, R01CA235412 (D.T.T.). F.K. was funded by the German Research Foundation (DFG; 466535590). R.A.B. was funded by NIH/NCI as well as K08CA248710. R.W.J. was supported by NIH K08CA226391. J.W.Z. was funded by Hopper-Belmont Foundation. M.V.M. was supported by NIH/NCI Grant R01CA238268.

## REFERENCES Uncategorized References

1. Park W, Chawla A, O'Reilly EM. Pancreatic Cancer: A Review. *JAMA* 2021;326(9):851–62 doi 10.1001/jama.2021.13027. [PubMed: 34547082]
2. Von Hoff DD, Ervin T, Arena FP, Chiorean EG, Infante J, Moore M, et al. Increased survival in pancreatic cancer with nab-paclitaxel plus gemcitabine. *N Engl J Med* 2013;369(18):1691–703 doi 10.1056/NEJMoa1304369. [PubMed: 24131140]
3. Conroy T, Desseigne F, Ychou M, Bouche O, Guimbaud R, Becouarn Y, et al. FOLFIRINOX versus gemcitabine for metastatic pancreatic cancer. *N Engl J Med* 2011;364(19):1817–25 doi 10.1056/NEJMoa1011923. [PubMed: 21561347]
4. Mizrahi JD, Surana R, Valle JW, Shroff RT. Pancreatic cancer. *Lancet* 2020;395(10242):2008–20 doi 10.1016/S0140-6736(20)30974-0. [PubMed: 32593337]
5. Hosein AN, Dougan SK, Aguirre AJ, Maitra A. Translational advances in pancreatic ductal adenocarcinoma therapy. *Nat Cancer* 2022;3(3):272–86 doi 10.1038/s43018-022-00349-2. [PubMed: 35352061]
6. Liudahl SM, Betts CB, Sivagnanam S, Morales-Oyarvide V, da Silva A, Yuan C, et al. Leukocyte Heterogeneity in Pancreatic Ductal Adenocarcinoma: Phenotypic and Spatial Features Associated with Clinical Outcome. *Cancer Discov* 2021;11(8):2014–31 doi 10.1158/2159-8290.CD-20-0841. [PubMed: 33727309]
7. Vayrynen SA, Zhang J, Yuan C, Vayrynen JP, Dias Costa A, Williams H, et al. Composition, Spatial Characteristics, and Prognostic Significance of Myeloid Cell Infiltration in Pancreatic Cancer. *Clin Cancer Res* 2021;27(4):1069–81 doi 10.1158/1078-0432.CCR-20-3141. [PubMed: 33262135]
8. Ohlund D, Elyada E, Tuveson D. Fibroblast heterogeneity in the cancer wound. *J Exp Med* 2014;211(8):1503–23 doi 10.1084/jem.20140692. [PubMed: 25071162]
9. Ohlund D, Handly-Santana A, Biffi G, Elyada E, Almeida AS, Ponz-Sarvisé M, et al. Distinct populations of inflammatory fibroblasts and myofibroblasts in pancreatic cancer. *J Exp Med* 2017;214(3):579–96 doi 10.1084/jem.20162024. [PubMed: 28232471]
10. Elyada E, Bolisetty M, Laise P, Flynn WF, Courtois ET, Burkhart RA, et al. Cross-Species Single-Cell Analysis of Pancreatic Ductal Adenocarcinoma Reveals Antigen-Presenting Cancer-Associated Fibroblasts. *Cancer Discov* 2019;9(8):1102–23 doi 10.1158/2159-8290.CD-19-0094. [PubMed: 31197017]
11. Huang H, Wang Z, Zhang Y, Pradhan RN, Ganguly D, Chandra R, et al. Mesothelial cell-derived antigen-presenting cancer-associated fibroblasts induce expansion of regulatory T cells in pancreatic cancer. *Cancer Cell* 2022;40(6):656–73 e7 doi 10.1016/j.ccell.2022.04.011. [PubMed: 35523176]
12. Francescone R, Barbosa Vendramini-Costa D, Franco-Barraza J, Wagner J, Muir A, Lau AN, et al. Netrin G1 Promotes Pancreatic Tumorigenesis through Cancer-Associated Fibroblast-Driven Nutritional Support and Immunosuppression. *Cancer Discov* 2021;11(2):446–79 doi 10.1158/2159-8290.CD-20-0775. [PubMed: 33127842]
13. Krishnamurthy AT, Shyer JA, Thai M, Gandham V, Buechler MB, Yang YA, et al. LRRRC15(+) myofibroblasts dictate the stromal setpoint to suppress tumour immunity. *Nature* 2022;611(7934):148–54 doi 10.1038/s41586-022-05272-1. [PubMed: 36171287]
14. Hingorani SR. Epithelial and stromal co-evolution and complicity in pancreatic cancer. *Nat Rev Cancer* 2023;23(2):57–77 doi 10.1038/s41568-022-00530-w. [PubMed: 36446904]
15. Ruffolo LI, Ullman NA, Dale B, Jackson KM, Burchard P, Georger M, et al. Antibody blockade of semaphorin 4D to sensitize pancreatic cancer to immune checkpoint blockade. *Journal of Clinical Oncology* 2020;38(5\_suppl):26- doi 10.1200/JCO.2020.38.5\_Supplementary26.
16. Mace TA, Shakya R, Pitarresi JR, Swanson B, McQuinn CW, Loftus S, et al. IL-6 and PD-L1 antibody blockade combination therapy reduces tumour progression in murine models of pancreatic cancer. *Gut* 2018;67(2):320–32 doi 10.1136/gutjnl-2016-311585. [PubMed: 27797936]
17. Zhang Y, Ware MB, Zaidi MY, Ruggieri AN, Olson BM, Komar H, et al. Heat Shock Protein-90 Inhibition Alters Activation of Pancreatic Stellate Cells and Enhances the Efficacy of PD-1 Blockade in Pancreatic Cancer. *Mol Cancer Ther* 2021;20(1):150–60 doi 10.1158/1535-7163.MCT-19-0911. [PubMed: 33037138]

18. Olive KP, Jacobetz MA, Davidson CJ, Gopinathan A, McIntyre D, Honess D, et al. Inhibition of Hedgehog signaling enhances delivery of chemotherapy in a mouse model of pancreatic cancer. *Science* 2009;324(5933):1457–61 doi 10.1126/science.1171362. [PubMed: 19460966]
19. Provenzano PP, Cuevas C, Chang AE, Goel VK, Von Hoff DD, Hingorani SR. Enzymatic targeting of the stroma ablates physical barriers to treatment of pancreatic ductal adenocarcinoma. *Cancer Cell* 2012;21(3):418–29 doi 10.1016/j.ccr.2012.01.007. [PubMed: 22439937]
20. Sahai E, Astsaturov I, Cukierman E, DeNardo DG, Egeblad M, Evans RM, et al. A framework for advancing our understanding of cancer-associated fibroblasts. *Nat Rev Cancer* 2020;20(3):174–86 doi 10.1038/s41568-019-0238-1. [PubMed: 31980749]
21. Xin L, Gao J, Zheng Z, Chen Y, Lv S, Zhao Z, et al. Fibroblast Activation Protein- $\alpha$  as a Target in the Bench-to-Bedside Diagnosis and Treatment of Tumors: A Narrative Review. *Front Oncol* 2021;11:648187 doi 10.3389/fonc.2021.648187. [PubMed: 34490078]
22. Aghajanian H, Kimura T, Rurik JG, Hancock AS, Leibowitz MS, Li L, et al. Targeting cardiac fibrosis with engineered T cells. *Nature* 2019;573(7774):430–3 doi 10.1038/s41586-019-1546-z. [PubMed: 31511695]
23. Tran E, Chinnasamy D, Yu Z, Morgan RA, Lee CC, Restifo NP, et al. Immune targeting of fibroblast activation protein triggers recognition of multipotent bone marrow stromal cells and cachexia. *J Exp Med* 2013;210(6):1125–35 doi 10.1084/jem.20130110. [PubMed: 23712432]
24. Kawase T, Yasui Y, Nishina S, Hara Y, Yanatori I, Tomiyama Y, et al. Fibroblast activation protein- $\alpha$ -expressing fibroblasts promote the progression of pancreatic ductal adenocarcinoma. *BMC Gastroenterol* 2015;15:109 doi 10.1186/s12876-015-0340-0. [PubMed: 26330349]
25. Young RM, Engel NW, Uslu U, Wellhausen N, June CH. Next-Generation CAR T-cell Therapies. *Cancer Discov* 2022;12(7):1625–33 doi 10.1158/2159-8290.CD-21-1683. [PubMed: 35417527]
26. Yeo D, Giardina C, Saxena P, Rasko JEJ. The next wave of cellular immunotherapies in pancreatic cancer. *Mol Ther Oncolytics* 2022;24:561–76 doi 10.1016/j.omto.2022.01.010. [PubMed: 35229033]
27. Morello A, Sadelain M, Adusumilli PS. Mesothelin-Targeted CARs: Driving T Cells to Solid Tumors. *Cancer Discov* 2016;6(2):133–46 doi 10.1158/2159-8290.CD-15-0583. [PubMed: 26503962]
28. Haas AR, Tanyi JL, O'Hara MH, Gladney WL, Lacey SF, Torigian DA, et al. Phase I Study of Lentiviral-Transduced Chimeric Antigen Receptor-Modified T Cells Recognizing Mesothelin in Advanced Solid Cancers. *Mol Ther* 2019;27(11):1919–29 doi 10.1016/j.ymthe.2019.07.015. [PubMed: 31420241]
29. Beatty GL, O'Hara MH, Lacey SF, Torigian DA, Nazimuddin F, Chen F, et al. Activity of Mesothelin-Specific Chimeric Antigen Receptor T Cells Against Pancreatic Carcinoma Metastases in a Phase I Trial. *Gastroenterology* 2018;155(1):29–32 doi 10.1053/j.gastro.2018.03.029. [PubMed: 29567081]
30. Larson RC, Maus MV. Recent advances and discoveries in the mechanisms and functions of CAR T cells. *Nat Rev Cancer* 2021;21(3):145–61 doi 10.1038/s41568-020-00323-z. [PubMed: 33483715]
31. Lee IK, Noguera-Ortega E, Xiao Z, Todd L, Scholler J, Song D, et al. Monitoring Therapeutic Response to Anti-Fibroblast Activation Protein (FAP) CAR T Cells using [18F]AlF-FAPI-74. *Clin Cancer Res* 2022 doi 10.1158/1078-0432.CCR-22-1379.
32. Bersani F, Lee J, Yu M, Morris R, Desai R, Ramaswamy S, et al. Bioengineered implantable scaffolds as a tool to study stromal-derived factors in metastatic cancer models. *Cancer Res* 2014;74(24):7229–38 doi 10.1158/0008-5472.CAN-14-1809. [PubMed: 25339351]
33. Delitto D, Pham K, Vlada AC, Sarosi GA, Thomas RM, Behrns KE, et al. Patient-derived xenograft models for pancreatic adenocarcinoma demonstrate retention of tumor morphology through incorporation of murine stromal elements. *Am J Pathol* 2015;185(5):1297–303 doi 10.1016/j.ajpath.2015.01.016. [PubMed: 25770474]
34. Baba T, Finetti P, Pancreatic Cancer G, Lillemoie KD, Warsaw AL, Fernandez-Del Castillo C, et al. A Lesson in Transcriptional Plasticity: Classical Identity Is Silenced, but Not Lost, in Pancreatic Ductal Adenocarcinoma Cell Lines. *Gastroenterology* 2022;163(5):1450–3 e3 doi 10.1053/j.gastro.2022.07.005. [PubMed: 35850199]

35. Scarfo I, Ormhoj M, Frigault MJ, Castano AP, Lorrey S, Bouffard AA, et al. Anti-CD37 chimeric antigen receptor T cells are active against B- and T-cell lymphomas. *Blood* 2018;132(14):1495–506 doi 10.1182/blood-2018-04-842708. [PubMed: 30089630]
36. Schmidts A, Ormhoj M, Choi BD, Taylor AO, Bouffard AA, Scarfo I, et al. Rational design of a trimeric APRIL-based CAR-binding domain enables efficient targeting of multiple myeloma. *Blood Adv* 2019;3(21):3248–60 doi 10.1182/bloodadvances.2019000703. [PubMed: 31698455]
37. Leick MB, Silva H, Scarfo I, Larson R, Choi BD, Bouffard AA, et al. Non-cleavable hinge enhances avidity and expansion of CAR-T cells for acute myeloid leukemia. *Cancer Cell* 2022;40(5):494–508 e5 doi 10.1016/j.ccell.2022.04.001. [PubMed: 35452603]
38. Larson RC, Kann MC, Bailey SR, Haradhvala NJ, Llopis PM, Bouffard AA, et al. CAR T cell killing requires the IFN $\gamma$  pathway in solid but not liquid tumours. *Nature* 2022;604(7906):563–70 doi 10.1038/s41586-022-04585-5. [PubMed: 35418687]
39. Choi BD, Yu X, Castano AP, Bouffard AA, Schmidts A, Larson RC, et al. CAR-T cells secreting BiTEs circumvent antigen escape without detectable toxicity. *Nat Biotechnol* 2019;37(9):1049–58 doi 10.1038/s41587-019-0192-1. [PubMed: 31332324]
40. Wang J, Saung MT, Li K, Fu J, Fujiwara K, Niu N, et al. CCR2/CCR5 inhibitor permits the radiation-induced effector T cell infiltration in pancreatic adenocarcinoma. *J Exp Med* 2022;219(5) doi 10.1084/jem.20211631.
41. Soares KC, Foley K, Olino K, Leubner A, Mayo SC, Jain A, et al. A preclinical murine model of hepatic metastases. *J Vis Exp* 2014(91):51677 doi 10.3791/51677. [PubMed: 25285458]
42. Yang T, Poenisch M, Khanal R, Hu Q, Dai Z, Li R, et al. Therapeutic HNF4A mRNA attenuates liver fibrosis in a preclinical model. *J Hepatol* 2021;75(6):1420–33 doi 10.1016/j.jhep.2021.08.011. [PubMed: 34453962]
43. Banik G, Betts CB, Liudahl SM, Sivagnanam S, Kawashima R, Cotechini T, et al. High-dimensional multiplexed immunohistochemical characterization of immune contexture in human cancers. *Methods Enzymol* 2020;635:1–20 doi 10.1016/bs.mie.2019.05.039. [PubMed: 32122539]
44. Boj SF, Hwang CI, Baker LA, Chio II, Engle DD, Corbo V, et al. Organoid models of human and mouse ductal pancreatic cancer. *Cell* 2015;160(1-2):324–38 doi 10.1016/j.cell.2014.12.021. [PubMed: 25557080]
45. Yang X, Lin Y, Shi Y, Li B, Liu W, Yin W, et al. FAP Promotes Immunosuppression by Cancer-Associated Fibroblasts in the Tumor Microenvironment via STAT3-CCL2 Signaling. *Cancer Res* 2016;76(14):4124–35 doi 10.1158/0008-5472.CAN-15-2973. [PubMed: 27216177]
46. Ligorio M, Sil S, Malagon-Lopez J, Nieman LT, Misale S, Di Pilato M, et al. Stromal Microenvironment Shapes the Intratumoral Architecture of Pancreatic Cancer. *Cell* 2019;178(1):160–75 e27 doi 10.1016/j.cell.2019.05.012. [PubMed: 31155233]
47. Oh SA, Li MO. TGF- $\beta$ : guardian of T cell function. *J Immunol* 2013;191(8):3973–9 doi 10.4049/jimmunol.1301843. [PubMed: 24098055]
48. Gundel B, Liu X, Lohr M, Heuchel R. Pancreatic Ductal Adenocarcinoma: Preclinical in vitro and ex vivo Models. *Front Cell Dev Biol* 2021;9:741162 doi 10.3389/fcell.2021.741162. [PubMed: 34746135]
49. Bareham B, Georgakopoulos N, Matas-Cespedes A, Curran M, Saeb-Parsy K. Modeling human tumor-immune environments in vivo for the preclinical assessment of immunotherapies. *Cancer Immunol Immunother* 2021;70(10):2737–50 doi 10.1007/s00262-021-02897-5. [PubMed: 33830275]
50. Adusumilli PS, Zauderer MG, Riviere I, Solomon SB, Rusch VW, O’Cearbhail RE, et al. A Phase I Trial of Regional Mesothelin-Targeted CAR T-cell Therapy in Patients with Malignant Pleural Disease, in Combination with the Anti-PD-1 Agent Pembrolizumab. *Cancer Discov* 2021;11(11):2748–63 doi 10.1158/2159-8290.CD-21-0407. [PubMed: 34266984]
51. Ebrahimi A, Cham J, Puglisi L, De Shadarevian M, Hermel DJ, Spierling Bagsic SR, et al. Do patients with metastatic pancreatic adenocarcinoma to the lung have improved survival? *Cancer Med* 2023;12(9):10243–53 doi 10.1002/cam4.5751. [PubMed: 36916531]
52. Nielsen SR, Quaranta V, Linford A, Emeagi P, Rainer C, Santos A, et al. Macrophage-secreted granulins support pancreatic cancer metastasis by inducing liver fibrosis. *Nat Cell Biol* 2016;18(5):549–60 doi 10.1038/ncb3340. [PubMed: 27088855]

53. Jenkins RW, Aref AR, Lizotte PH, Ivanova E, Stinson S, Zhou CW, et al. Ex Vivo Profiling of PD-1 Blockade Using Organotypic Tumor Spheroids. *Cancer Discov* 2018;8(2):196–215 doi 10.1158/2159-8290.CD-17-0833. [PubMed: 29101162]
54. Kraman M, Bambrough PJ, Arnold JN, Roberts EW, Magiera L, Jones JO, et al. Suppression of antitumor immunity by stromal cells expressing fibroblast activation protein- $\alpha$ . *Science* 2010;330(6005):827–30 doi 10.1126/science.1195300. [PubMed: 21051638]
55. Feig C, Jones JO, Kraman M, Wells RJ, Deonarine A, Chan DS, et al. Targeting CXCL12 from FAP-expressing carcinoma-associated fibroblasts synergizes with anti-PD-L1 immunotherapy in pancreatic cancer. *Proc Natl Acad Sci U S A* 2013;110(50):20212–7 doi 10.1073/pnas.1320318110. [PubMed: 24277834]
56. Qi J, Sun H, Zhang Y, Wang Z, Xun Z, Li Z, et al. Single-cell and spatial analysis reveal interaction of FAP(+) fibroblasts and SPP1(+) macrophages in colorectal cancer. *Nat Commun* 2022;13(1):1742 doi 10.1038/s41467-022-29366-6. [PubMed: 35365629]
57. Korell F, Berger TR, Maus MV. Understanding CAR T cell-tumor interactions: Paving the way for successful clinical outcomes. *Med (N Y)* 2022;3(8):538–64 doi 10.1016/j.medj.2022.05.001.
58. Ho WJ, Jaffee EM, Zheng L. The tumour microenvironment in pancreatic cancer - clinical challenges and opportunities. *Nat Rev Clin Oncol* 2020;17(9):527–40 doi 10.1038/s41571-020-0363-5. [PubMed: 32398706]
59. Knelson EH, Ivanova EV, Tarannum M, Campisi M, Lizotte PH, Booker MA, et al. Activation of Tumor-Cell STING Primes NK-Cell Therapy. *Cancer Immunol Res* 2022;10(8):947–61 doi 10.1158/2326-6066.CIR-22-0017. [PubMed: 35678717]
60. Liu Y, Sun Y, Wang P, Li S, Dong Y, Zhou M, et al. FAP-targeted CAR-T suppresses MDSCs recruitment to improve the antitumor efficacy of claudin18.2-targeted CAR-T against pancreatic cancer. *J Transl Med* 2023;21(1):255 doi 10.1186/s12967-023-04080-z. [PubMed: 37046312]
61. Sakemura R, Hefazi M, Siegler EL, Cox MJ, Larson DP, Hansen MJ, et al. Targeting cancer-associated fibroblasts in the bone marrow prevents resistance to CART-cell therapy in multiple myeloma. *Blood* 2022;139(26):3708–21 doi 10.1182/blood.2021012811. [PubMed: 35090171]
62. Seppala TT, Zimmerman JW, Suri R, Zlomke H, Ivey GD, Szabolcs A, et al. Precision Medicine in Pancreatic Cancer: Patient-Derived Organoid Pharmacotyping Is a Predictive Biomarker of Clinical Treatment Response. *Clin Cancer Res* 2022;28(15):3296–307 doi 10.1158/1078-0432.CCR-21-4165. [PubMed: 35363262]
63. Dekkers JF, Alieva M, Cleven A, Keramati F, Wezenaar AKL, van Vliet EJ, et al. Uncovering the mode of action of engineered T cells in patient cancer organoids. *Nature Biotechnology* 2022 doi 10.1038/s41587-022-01397-w.
64. Thommen DS, Schumacher TN. T Cell Dysfunction in Cancer. *Cancer Cell* 2018;33(4):547–62 doi 10.1016/j.ccell.2018.03.012. [PubMed: 29634943]
65. Cohen SJ, Alpaugh RK, Palazzo I, Meropol NJ, Rogatko A, Xu Z, et al. Fibroblast activation protein and its relationship to clinical outcome in pancreatic adenocarcinoma. *Pancreas* 2008;37(2):154–8 doi 10.1097/MPA.0b013e31816618ce. [PubMed: 18665076]
66. Bughda R, Dimou P, D'Souza RR, Klampatsa A. Fibroblast Activation Protein (FAP)-Targeted CAR-T Cells: Launching an Attack on Tumor Stroma. *Immunotargets Ther* 2021;10:313–23 doi 10.2147/ITT.S291767. [PubMed: 34386436]
67. Waghray M, Yalamanchili M, Dziubinski M, Zeinali M, Erkkinen M, Yang H, et al. GM-CSF Mediates Mesenchymal-Epithelial Cross-talk in Pancreatic Cancer. *Cancer Discov* 2016;6(8):886–99 doi 10.1158/2159-8290.CD-15-0947. [PubMed: 27184426]
68. Good CR, Aznar MA, Kuramitsu S, Samareh P, Agarwal S, Donahue G, et al. An NK-like CAR T cell transition in CAR T cell dysfunction. *Cell* 2021;184(25):6081–100 e26 doi 10.1016/j.cell.2021.11.016. [PubMed: 34861191]
69. Klampatsa A, Dimou V, Albelda SM. Mesothelin-targeted CAR-T cell therapy for solid tumors. *Expert Opin Biol Ther* 2021;21(4):473–86 doi 10.1080/14712598.2021.1843628. [PubMed: 33176519]
70. Maus MV, Haas AR, Beatty GL, Albelda SM, Levine BL, Liu X, et al. T cells expressing chimeric antigen receptors can cause anaphylaxis in humans. *Cancer Immunol Res* 2013;1:26–31. [PubMed: 24777247]

71. Beatty GL, Haas AR, Maus MV, Torigian DA, Soulen MC, Plesa G, et al. Mesothelin-specific chimeric antigen receptor mRNA-engineered T cells induce anti-tumor activity in solid malignancies. *Cancer Immunol Res* 2014;2(2):112–20 doi 10.1158/2326-6066.CIR-13-0170. [PubMed: 24579088]
72. Wang LC, Lo A, Scholler J, Sun J, Majumdar RS, Kapoor V, et al. Targeting fibroblast activation protein in tumor stroma with chimeric antigen receptor T cells can inhibit tumor growth and augment host immunity without severe toxicity. *Cancer Immunol Res* 2014;2(2):154–66 doi 10.1158/2326-6066.CIR-13-0027. [PubMed: 24778279]
73. Kakarla S, Chow KK, Mata M, Shaffer DR, Song XT, Wu MF, et al. Antitumor effects of chimeric receptor engineered human T cells directed to tumor stroma. *Mol Ther* 2013;21(8):1611–20 doi 10.1038/mt.2013.110. [PubMed: 23732988]
74. Lo A, Wang LS, Scholler J, Monslow J, Avery D, Newick K, et al. Tumor-Promoting Desmoplasia Is Disrupted by Depleting FAP-Expressing Stromal Cells. *Cancer Res* 2015;75(14):2800–10 doi 10.1158/0008-5472.CAN-14-3041. [PubMed: 25979873]
75. Hofheinz RD, al-Batran SE, Hartmann F, Hartung G, Jager D, Renner C, et al. Stromal antigen targeting by a humanised monoclonal antibody: an early phase II trial of sibiruzumab in patients with metastatic colorectal cancer. *Onkologie* 2003;26(1):44–8 doi 10.1159/000069863. [PubMed: 12624517]
76. Curioni A, Britschgi C, Hiltbrunner S, Bankel L, Gulati P, Weder W, et al. 1226P - A phase I clinical trial of malignant pleural mesothelioma treated with locally delivered autologous anti-FAP-targeted CAR T-cells. *Annals of Oncology* 2019;30:v501 doi 10.1093/annonc/mdz253.052.
77. Melero I, Tanos T, Bustamante M, Sanmamed MF, Calvo E, Moreno I, et al. A first-in-human study of the fibroblast activation protein-targeted, 4-1BB agonist RO7122290 in patients with advanced solid tumors. *Sci Transl Med* 2023;15(695):eabp9229 doi 10.1126/scitranslmed.abp9229. [PubMed: 37163618]
78. Nishio T, Koyama Y, Liu X, Rosenthal SB, Yamamoto G, Fujii H, et al. Immunotherapy-based targeting of MSLN(+) activated portal fibroblasts is a strategy for treatment of cholestatic liver fibrosis. *Proc Natl Acad Sci U S A* 2021;118(29) doi 10.1073/pnas.2101270118.

**Translational Relevance:**

Pancreatic ductal adenocarcinoma (PDAC) is historically difficult to treat, with poor outcomes. CAR T cells are a promising treatment option for PDAC due to their ability to track down and eliminate cancer cells. However, CAR T cells have yet to reach their full potential in solid tumors, in part due to suppression by the tumor microenvironment (TME). Here, we generated CAR T cells targeting a PDAC-associated antigen (mesothelin) that also secrete a T-cell engaging antibody molecule (TEAM) to fibroblast activation protein (FAP) and CD3 (termed meso<sup>FAP</sup> CAR-TEAM cells) to target cancer-associated fibroblasts (CAFs) in the TME by engaging T cells. These CAR-TEAM cells successfully eliminated PDAC and CAFs in several in vitro, in vivo, and ex vivo patient-derived models, demonstrating their potential benefit in treating patients with PDAC. Given these results, we aim to initiate a clinical trial of meso<sup>FAP</sup> CAR-TEAM cells to primarily determine their safety in patients with efficacy as a secondary endpoint.

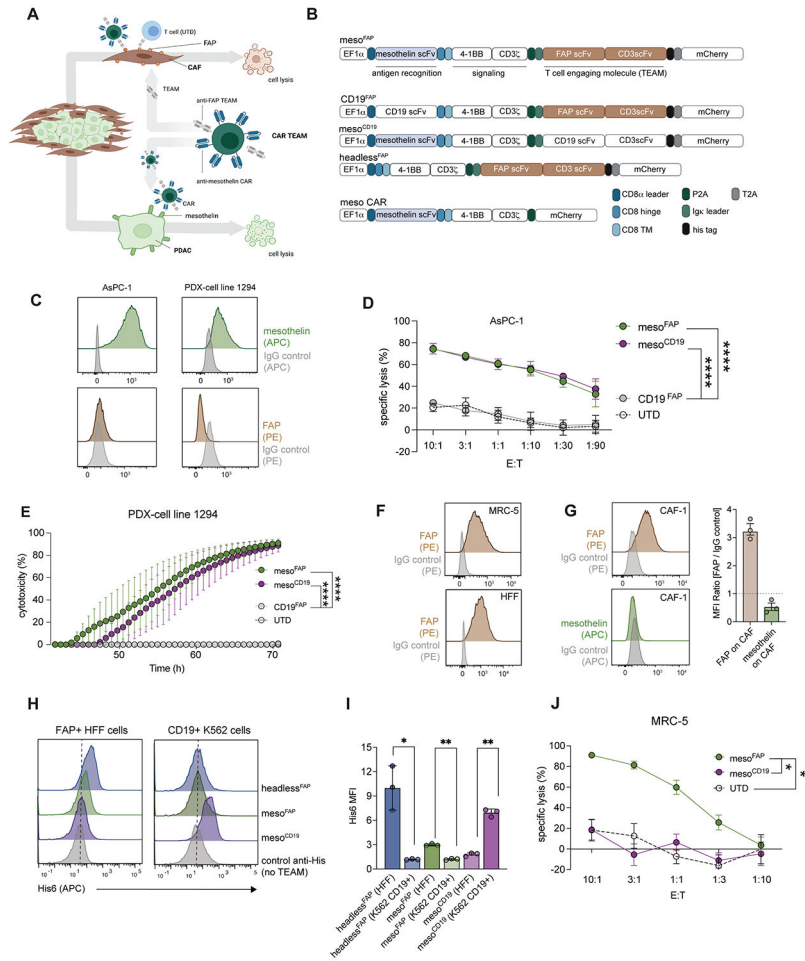


**Figure 1. Meso<sup>FAP</sup> CAR T-cells specifically recognize their target antigens and eliminate mesothelin-expressing PDAC cells and FAP-expressing fibroblasts.**  
**A.** Schematic of meso<sup>FAP</sup> CAR T-cells targeting PDAC and CAFs (created with [BioRender.com](https://www.biorender.com)). **B.** Graphic representation constructs used to make TEAM-secreting CAR T-cells. **C.** Representative histograms of flow cytometric analysis of mesothelin and FAP expression on PDAC cell lines, AsPC-1 and PDX-1294. **D-E.** CAR<sup>TEAM</sup> cytotoxicity against AsPC-1 and PDX-1294 assessed by **(D)** a luciferase-based specific lysis assay and **(E)** a real-time impedance-based assay. **F.** Representative histograms of flow cytometric analysis of FAP expression on the fibroblast-cell line MRC-5 and HFF. **G.** Representative histograms including bar graph of flow cytometric analysis of FAP and mesothelin expression on CAF-1. **H-I.** Flow cytometric detection of His tag on TEAMs that recognize their specific target antigen on FAP+ HFF cells or CD19+ K562 cells. **J.** CAR<sup>TEAM</sup> cytotoxicity against MRC-5 assessed by a luciferase-based specific lysis assay. All data represent mean  $\pm$  SEM and are representative of at least 3 independent experiments. Stars indicate significance between biological triplicates using a two-tailed *t*-test at the 10:1 ratio (panels D and I), and one-way ANOVA with Dunnett’s multiple comparison post hoc analysis (panel E), or HFF vs. K562 (panel H). \**p*<0.05, \*\**p*<0.01, \*\*\*\**p*<0.0001, E:T = effector to target ratio. PDAC: pancreatic ductal adenocarcinoma, CAF: cancer-associated fibroblasts, UTD: untransduced T-cell.

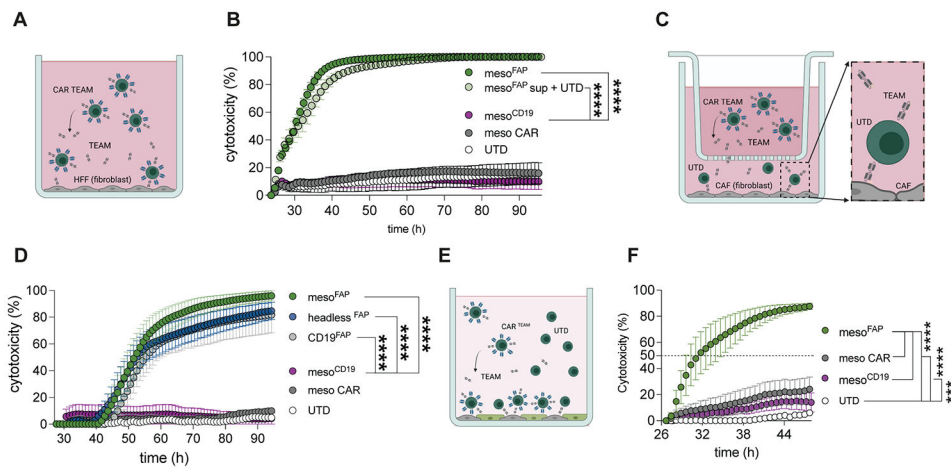


**Figure 2. Meso<sup>FAP</sup> CAR T-cells or UTD mixed with FAP TEAM specifically eliminate FAP-expressing fibroblasts and are superior to CARs targeting mesothelin only in PDAC + CAF co-cultures.**

**A.** Schematic of meso<sup>FAP</sup> CAR T-cells targeting HFF fibroblasts. **B.** Real-time impedance-based cytotoxicity assay of sorted CAR<sup>TEAM</sup> or UTDs with supernatant from meso<sup>FAP</sup> CAR T-cells against FAP-expressing HFF using an effector to target ratio (E:T) of 1:1. **C.** Schematic of transwell system containing UTDs and CAFs in the bottom well and TEAM-secreting CAR T-cells in the upper well. **D.** Real-time impedance-based cytotoxicity assay of sorted CAR<sup>TEAM</sup> in the transwell system with CAF-1 and UTD cells in the lower well, E:T = 1:1. **E.** Schematic of co-culture system containing target-cells CAF-1 and AsPC-1 in a 1:1 ratio treated with CAR or UTD as effector cells (E:T = 1:5 = 0.2 CAR : (1 CAF : 1 PDAC)). **F.** Real-time impedance-based killing assay in the co-culture system (CAF1 and AsPC-1 in 1:1 ratio) treated with meso<sup>FAP</sup>, meso<sup>CD19</sup>, or anti-mesothelin CAR T-cells or UTD controls. All data are plotted as the mean  $\pm$  SEM. Stars indicate significance between biological triplicates assessed by one-way ANOVA and Dunnett's multiple comparison post hoc analysis. \*\*\* $p < 0.001$ , \*\*\*\* $p < 0.0001$ . PDAC: pancreatic ductal adenocarcinoma, CAF: cancer-associated fibroblasts, UTD: untransduced T-cell. Schematics were created with [BioRender.com](https://www.biorender.com).

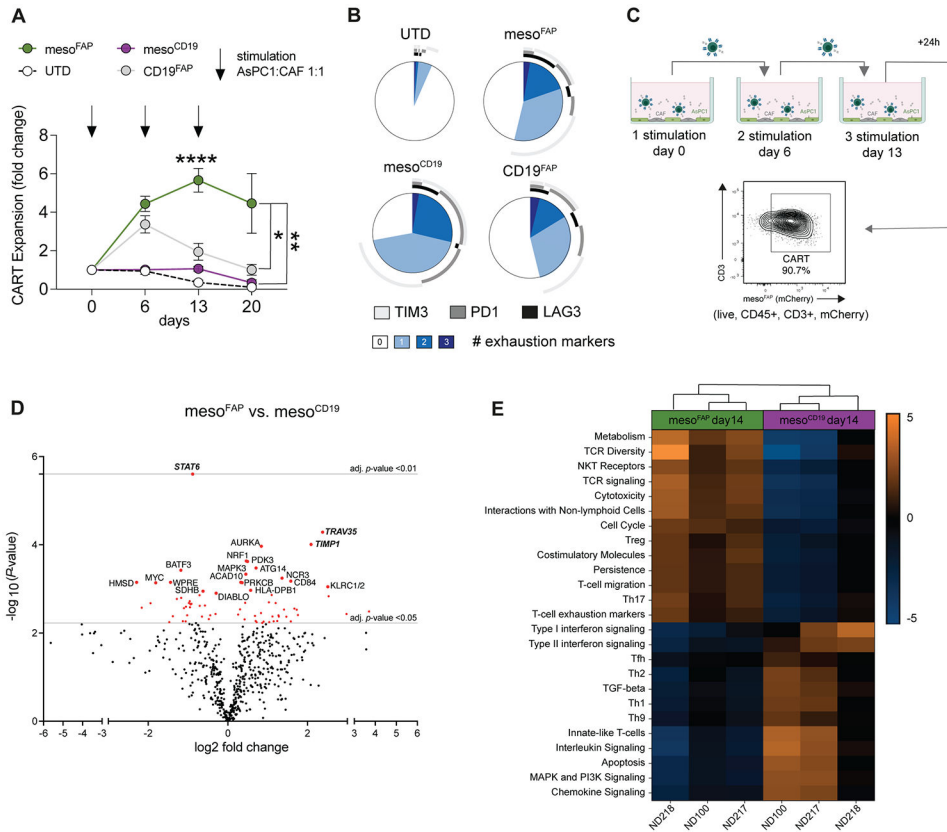


**Figure 3. Meso<sup>FAP</sup> proliferate more in the presence of PDAC and CAF and demonstrate a different activation profile than control CAR T-cells.**

**A.** Fold change in T-cell expansion when CAR<sup>TEAM</sup> or UTD were repeatedly stimulated with AsPC-1 and CAF-1. (AsPC-1:CAF-1:T-cell ratio of 1:1:2). **B.** Exhaustion markers expressed by T-cells in the co-culture at day 13 as measured by flow cytometry. Data is from one representative donor. **C.** Schematic of co-culture set-up (created with BioRender.com). T-cells (live, CD45+, CD3+, and mCherry+) were sorted 24h after the 3rd stimulation (day 14) and RNA analysis was performed by NanoString. **D.** Volcano plot of differential RNA expression of flowcytometric sorted (expressing the same level of mCherry) meso<sup>FAP</sup> CAR T-cells versus meso<sup>CD19</sup> CAR T-cells following co-culture with AsPC-1 and CAFs. The top 20 genes are annotated. The grey horizontal line indicates an adjusted p-value of 0.05 and 0.001. **E.** Pathway analysis of NanoString data comparing meso<sup>FAP</sup> and meso<sup>CD19</sup> CAR T-cells from 3 independent healthy donors (ND218, ND210, and ND100). All data represent mean  $\pm$  SEM of at least biological triplicates. MFI-sorted CAR T cells or UTDs were added in biological triplicates per condition. Stars indicate significance as determined by one-way ANOVA and Dunnett's multiple comparison post hoc analysis. \* $p < 0.05$ , \*\* $p < 0.01$ , \*\*\* $p < 0.001$ , \*\*\*\* $p < 0.0001$ , E:T = effector to target ratio. PDAC: pancreatic ductal adenocarcinoma, CAF: cancer-associated fibroblasts, UTD: untransduced T-cell, TEMRA: T-effector memory and CD45+/CCR7- subset, ND: normal donor.

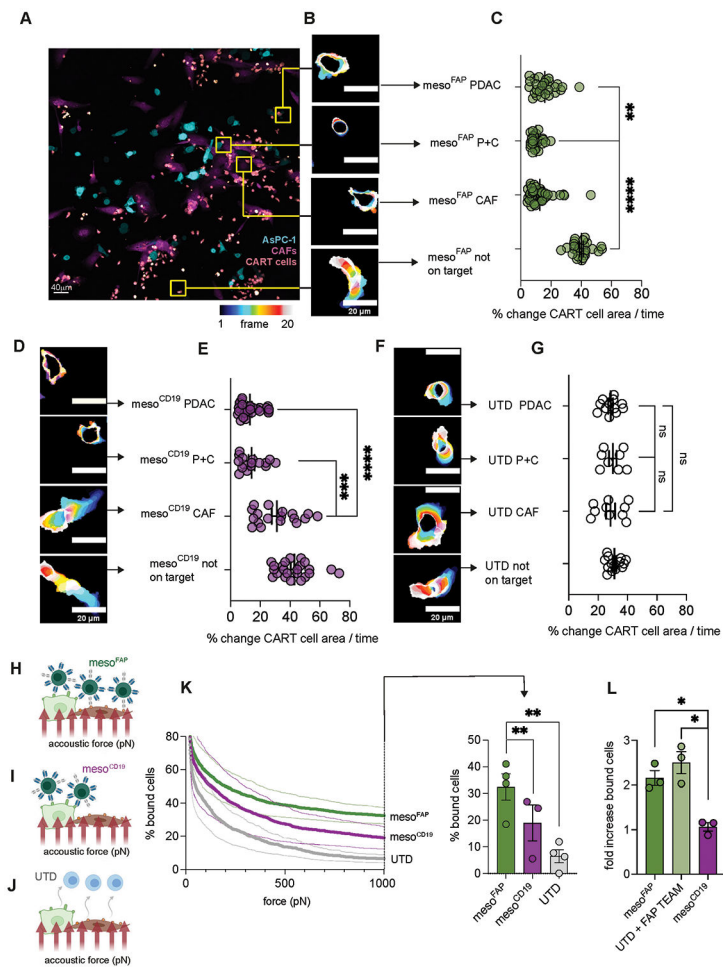


**Figure 4. Live cell, time-lapse microscopy shows reduced edge dynamics and acoustic force microscopy reveals increased binding avidity of meso<sup>FAP</sup> in comparison to controls.**

**A.** Representative image of sorted meso<sup>FAP</sup> CAR T-cells (pink/salmon) interacting with AsPC-1 (cyan), CAFs (magenta), or AsPC-1 and CAFs. **B.** Representative images visualizing edge dynamics (percentage change of CAR T-cell area over time) of meso<sup>FAP</sup> CAR T-cells over 20 frames (frame 1 dark blue to frame 20 white). **C.** Percentage change of meso<sup>FAP</sup> CAR T-cell area over time (number of cell interactions counted: PDAC, n=28; P+C, n=25; CAF, n=42; not on target, n=25). **D,F.** Representative images visualizing edge dynamics of **D.** meso<sup>CD19</sup> CAR T-cells or **F.** UTD T-cells. **E,G.** Percentage change of **E.** meso<sup>CD19</sup> CAR T-cells over time (number of cell interactions counted: PDAC, n=28; P+C, n=16; CAF, n=18; not on target, n=23) or **G.** UTDs over time (number of cell interactions counted: PDAC n=12; P+C, n=8; CAF, n=10; not on target, n=14). **H-J.** Schematic showing 1:1 ratio of AsPC-1 and CAFs in the flow chamber to measure cell binding of meso<sup>FAP</sup> (**H**), meso<sup>CD19</sup> (**I**), and UTD (**J**) avidity by acoustic force microscopy (created with [BioRender.com](https://www.biorender.com)). **K.** Percentage of meso<sup>FAP</sup>, meso<sup>CD19</sup>, or UTD bound to 1:1 AsPC-1 and CAF mixture (left) with an increasing amount of acoustic force (pN) and (right) at 1000pN as measured by z-Movi. **L.** Fold increase of bound meso<sup>FAP</sup> CAR T-cells or UTD cells with the addition of FAP-TEAM on HFF fibroblasts using z-Movi. All data represent mean +/-SEM. Representative images have been chosen within 1 standard deviation from the

median. Results were obtained from biological duplicates, from at least 3 different locations on the slide. Stars represent significance as determined by unpaired two-tailed t-tests. \* $p < 0.05$ , \*\* $p < 0.01$  \*\*\* $p < 0.001$  \*\*\*\* $p < 0.0001$ . UTD: untransduced T-cell, pN: picoNewton, P+C: PDAC+CAF.

Author Manuscript

Author Manuscript

Author Manuscript

Author Manuscript

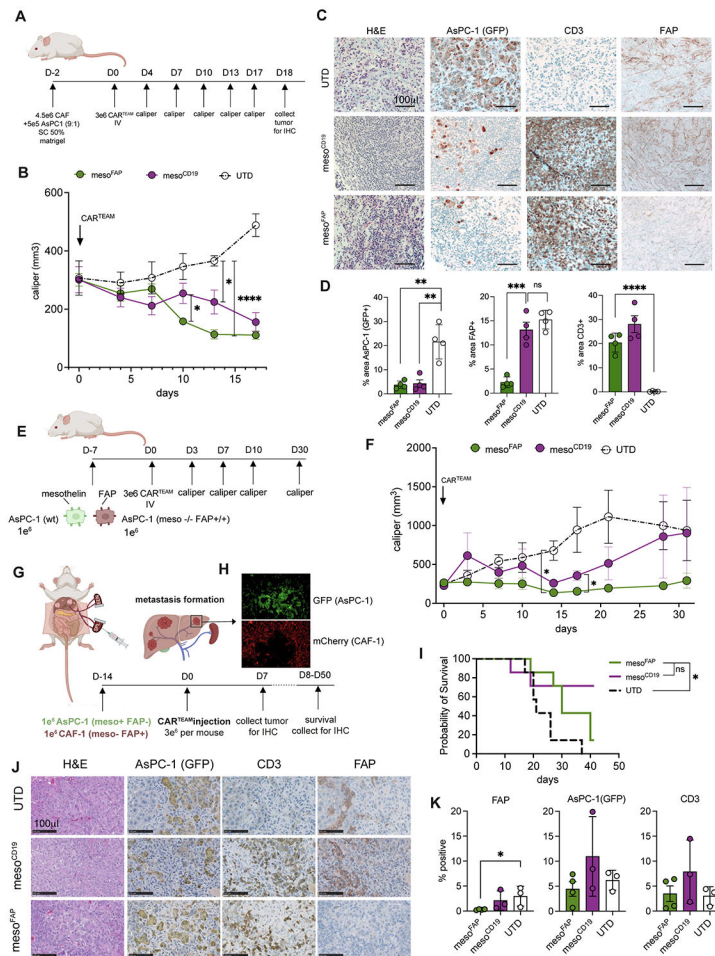


**Figure 5. meso<sup>FAP</sup> CAR T-cells are efficacious against PDAC and CAFs in vivo.**

**A.** Schematic of experimental setup in which CAF-1 and AsPC-1 (9:1 ratio) were subcutaneously implanted in the flank of NSG mice. Mice were treated intravenously with UTD, meso<sup>FAP</sup>, or meso<sup>CD19</sup> CAR T-cells 2 days after tumor-CAF implantation. **B.** Tumor volume over time as measured by caliper. **C.** Representative hematoxylin and eosin (H&E) staining and immunohistochemical (IHC) staining for GFP (AsPC-1), and CD3 (T-cells) on tumors harvested on day 18 from mice treated with UTD, meso<sup>CD19</sup> or meso<sup>FAP</sup> CAR T-cells. **D.** Quantification of **C** as % area positive for each marker. **E.** Schematic of experimental setup with AsPC-1 and AsPC-1 mesothelin <sup>-/-</sup> FAP<sup>+</sup> in a 1:1 ratio being subcutaneously implanted into the flank of NSG mice. Mice were treated intravenously with UTD, meso<sup>FAP</sup>, or meso<sup>CD19</sup> CAR T-cells 7 days after tumor implantation. **F.** Tumor volume over time as measured by caliper. **G.** Schematic of experimental hemi-spleen model for liver metastasis. **H.** Representative immunofluorescence images of PDAC (AsPC-1 GFP<sup>+</sup>) and CAFs (mCherry<sup>+</sup>) metastasis in murine liver. **I.** Kaplan-Meier curve of survival cohort of mice (n=7 mice carried out through death). **J.** IHC representation of sequential cut slides from liver metastasis from mice sacrificed on day 21. **K.** Quantification of **J** as percent positive cell for each marker (n=3). Data represent mean +/- SEM. Stars indicate significance as determined by unpaired two-tailed *t*-tests. \**p* < 0.05, \*\**p* < 0.01, \*\*\**p*

< 0.001, \*\*\*\* $p < 0.0001$  (panels **D** and **K**). N=4-5 animals/group, repeated with T-cells from two healthy donors. Data represent two-way ANOVA with correction for multiple comparisons, individual p-values are indicated \* $p < 0.05$ , \*\*\*\* $p < 0.0001$  (panel **B** and **F**). Data represent survival analysis (Kaplan-Meier) individual p-values are indicated \* $p < 0.05$ , ns = not significant (panel **I**). Schematics were created with [BioRender.com](https://www.biorender.com).

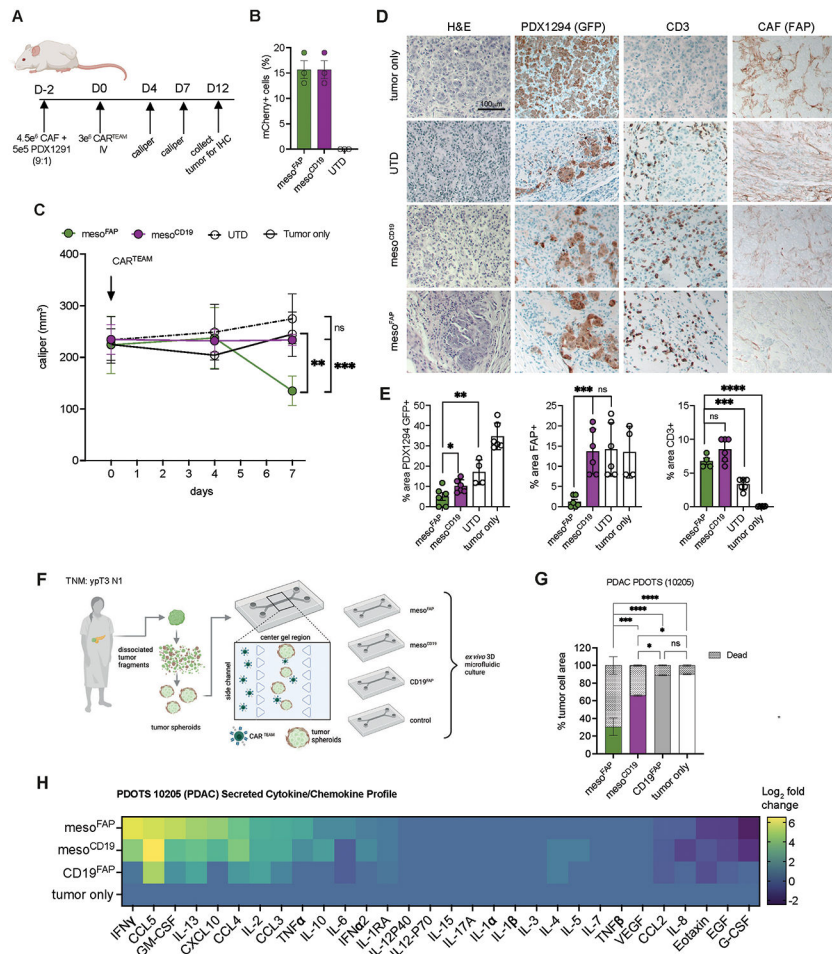


**Figure 6. Meso<sup>FAP</sup> CAR T-cells outperform control CAR T-cells in PDX *in vivo* and *ex vivo* models.**

**A.** Schematic of experimental design in which CAFs and PDX1291 cell line (9:1 ratio) were subcutaneously implanted in the flank of NSG mice. Mice were treated intravenously on day 2 post-tumor-CAF implantation with UTD, meso<sup>FAP</sup>, and meso<sup>CD19</sup> CAR T-cells. **B.** Transduction efficiencies of normalized CAR<sup>TEAM</sup> including UTD of *in vivo* experiment from 3 independent experiments. **C.** Tumor volume over time as measured by caliper (n=5 mice per group). **D.** Representative hematoxylin and eosin (H&E) staining and immunohistochemical (IHC) staining for GFP (PDX1294), FAP (CAF), and CD3 (T-cells) on tumors harvested on day 14. Scale bar indicates 100mm. **E.** Quantification of **D.** as percent area positive for each marker; 4-6 representative examples quantified. **F.** Schematic of PDOTS experimental setup including the 3D microfluidic co-culture system with a side channel (where CAR<sup>TEAM</sup> are added with an E:T of 1:3) and center/gel region (where tumor spheroids are grown in collagen hydrogels). **G.** Evaluation of live/dead cells on day 5 of meso<sup>FAP</sup>-, meso<sup>CD19</sup>-, and CD19<sup>FAP</sup>-treated or tumor-only PDOTS (n=3). **H.** Secreted cytokine and chemokines analysis as Log<sub>2</sub> fold change (relative to control samples) on day 5 of meso<sup>FAP</sup>, meso<sup>CD19</sup>, CD19<sup>FAP</sup>, and tumor-only PDOTS from F. Data represents mean +/- SEM. Stars indicate significance as determined by unpaired two-tailed *t*-tests (panels B and D) or one-way ANOVA with Tukey's multiple comparisons test (panel F). \**p* < 0.05,

\*\* $p < 0.01$  \*\*\* $p < 0.001$  \*\*\*\* $p < 0.0001$ , ns: not significant. Schematics were created with [BioRender.com](https://BioRender.com).

Author Manuscript

Author Manuscript

Author Manuscript

Author Manuscript

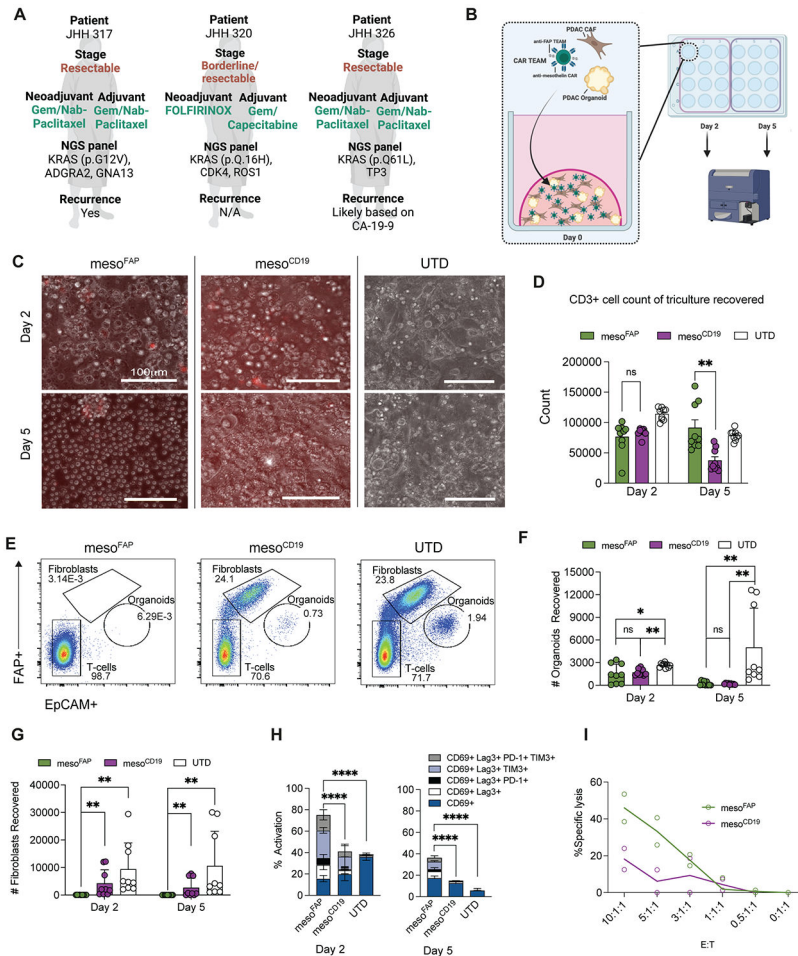


**Figure 7. Efficacy of meso<sup>FAP</sup> CAR T-cell in patient-derived organoids (PDO) with matching CAFs.**

**A.** PDAC patient information corresponding to PDO and CAF co-cultures. **B.** Schematic of meso<sup>FAP</sup> CAR T-cells targeting organoid co-cultures consisting of PDAC PDO and CAF. **C.** Co-culture transillumination at day 2 and day 5 of co-culture visualized by Nikon ECLIPSE Ti2 microscope at 20X. Transillumination and RPF images merged by NIS-Elements AR Software. **D.** CD3+ recovery acquired at both day 2 and day 5. **E.** Representative flow cytometry plots of specific cytotoxicity of meso<sup>FAP</sup> targeting JHH317 FAP+ CAF and PDO co-culture at day 5. **F.** Flow cytometric analysis showing PDO count recovered on day 2 and day 5. **G.** Flow cytometric analysis showing CAF count recovered on day 2 and day 5. **H.** Flow cytometric analysis of activation and exhaustion markers on CD3+ CART-cells at day 2 and day 5. **I.** VITAL CTL killing assay of target PDO with CAR T effector cells, and UTD T-cells in increasing ratios of effector : target/T cells (technical duplicate; unpaired, two-tailed *t*-test, *p*=0.09 at 10:1:1 ratio). Data represent means of biological and technical triplicates. Stars indicate significance as determined by Wilcoxon test (panels D, F, and G) or paired, two-tailed *t*-test (panel H and I). \**p* < 0.05, \*\*\*\**p* < 0.0001. PDO: pancreatic ductal adenocarcinoma organoids, Dx: diagnosis, NGS: next-generation sequencing. Schematics were created with [BioRender.com](https://www.biorender.com).